DIVISION OF ENGINEERING RESEARCH AND DEVELOPME
DEPARTMENT OF ELECTRICAL ENGINEERING

Thin Cylindrical Ceramic Transducer

by N. T. CHIEU and F. H. MIDDLETON

Technical Report No. 6

Sponsor: Office of Naval Research
Acoustics Programs, Code 468
Contract: Nonr 396(12)
Authority: NR 185-700/8-18-64
Project: RR 001-03-05

UNIVERSITY OF RHODE ISLAND
KINGSTON, RHODE ISLAND

University of Rhode Island

Division of Engineering Research and Development

Electrical Engineering Department

Technical Report No. 6

THIN CYLINDRICAL CERAMIC TRANSDUCERS

by

N. T. Chieu

Research Assistant

and

F. H. Middleton

Professor

Sponsor: Office of Naval Research
Acoustics Programs, Code 468
Contract: Nonr 396(12)
Date: October 1, 1964

ABSTRACT

Free-flooded thin cylindrical ceramic rings have distinct advantages in deep water transducer applications. Their actual behavior in different resonance modes is not well known. To study this problem an extensive review of the existing theories on the finite cylinder has been made, the advantages and disadvantages of each pointed out. Moreover, four model rings are used in the laboratory to study the problem experimentally. Ring pairs of 1.25" and 1" in diameter are identical except for heights which range from 5" to 0.5". The frequency range is from 10 kc to 200 kc. The pulse technique is used and the results include response characteristics, impedance curves, radiation patterns and power output characteristics for both the free-flooded and air-backed arrangements. The same ring is used for flooded and pressure-relieved experiments so that there are no extraneous differences in the two cases. This is accomplished by means of a very thin membrane cemented to each end of the ring. The compliance of the membrane is so large that mechanical effects on the ring itself are negligible.

TABLE OF CONTENTS

		Page.
I	INTRODUCTION	1
II	REVIEW OF THEORETICAL STUDIES OF RINGS	5
	1. Model Radiator Extended by Two Semi-Infinite, Rigid Cylindrical Baffles	5
	2. Method Using Series Of Spherical Wave Harmonics	8
	3. Finite-difference Method.	10
	4. Variational Principle For Radiation Loading	11
	5. Iteration Technique For Cylindrical Radiator Problem. . .	13
III	RESULT OF OTHER EXPERIMENTAL STUDIES	15
IV	RING DESIGN PARAMETER STUDY.	17
	1. Instrumentation	18
	[a] The Tank.	18
	[b] The Driving Mechanism	18
	[c] The Electronic Equipment.	19
	2. Absolute Calibration Of Transducers	23
	3. Experimental Procedure.	28
V	DISCUSSION OF RESULTS.	62
VI	CONCLUSIONS.	70
VII	APPENDIX	72
VIII	REFERENCES	74

LIST OF FIGURES

FIGURE		Page.
1	Block Diagram Of Driving Mechanism	20
2	Diagram Of Transmitter Gate	22
3	Block Diagram Of Electronic Arrangement	24
4	CRT Photograph Of 37 KC Signal	30
5	CRT Photograph Of 74 KC Signal	31
6	Circuit Diagram For Transducer Impedance Plottings	32
7a	A: Impedance Curves And Receiving Characteristics	33
7b	B: Impedance Curves And Receiving Characteristics	34
7c	C: Impedance Curves And Receiving Characteristics	35
7d	D: Impedance Curves And Receiving Characteristics	36
8a	Transfer Characteristics Of A-B System	38
8a'	Transfer Characteristics Of A-C System	39
8b	Transfer Characteristics Of B-C System	40
8c	Transfer Characteristics Of C-B System	41
8d	Transfer Characteristics Of D-B System	42
9a	Transmitting Response Of Transducers A And B	43
9b	Transmitting Response Of Transducers C And D	44
10	Patterns For ka = 2 of Transducers A and D	46
11	Patterns For ka = 2 Of Transducers B And C	47
12	Patterns For ka = 3 Of Transducers A And D	48
13	Patterns For ka = 3 Of Transducers B And C	49
14	Free-Flooded Patterns For Small Frequency Change	50

LIST OF FIGURES cont'd

15 Free-Flooded Patterns For Small Frequency Change 51

16 Patterns For Small Frequency Change 52

17 Patterns For ka = 3.5 Of Transducers A, C And D 53

18 Patterns For ka = 4 Of Transducers B And C 54

19 Patterns For ka = 4.2 Of Transducers A and B 55

20 Patterns For ka at And Near 5 Of Transducers A And B 56

21 Patterns For ka at And Near 6 Of Transducers A And C 57

22 Patterns For ka at And Near 7 Of Transducers A 58

23 Patterns For ka = 6.5 Of Transducers A And D 59

24 Length Mode Of Transducers B And C 60

LIST OF TABLES

TABLE		Page.
I	Total Power Output Of Ceramic Transducers	61
II	Squirter Resonances	64

I

INTRODUCTION

This report is on a continuing study of the "barrel-stave" flooded cylindrical acoustic radiator. This transducer has been highly successful in deep ocean work, and yet there remain several important questions concerning its behavior. The main problem lies in the face that its shape does not lend itself well to mathematical representation. It is essentially a short cylinder compared to its diameter, and in operation, both the inside and outside cylindrical surfaces are important to the net radiated field.

These outstanding questions have not prevented successful design of the radiators and indeed, the high conversion efficiencies obtained in practice make it even more desirable to understand their basic operation. In particular, this study considers the large cylinder whose diameter is the order of several feet, and whose height is a foot or two. The fundamental circumferential resonance is thus below 1000 cps.

In the early part of this report the various methods of analytically dealing with the finite cylindrical radiator will be presented briefly and they will be compared with each other. The method of R. S. Haas and F. H. Middleton will be given special attention because of a considerable amount of computer results produced in that previous study. In a later section of the report these computer results are compared with the experi-

mental model measurements obtained in the present study.

If the performance of the large cylinder were well understood, it would be possible to predict the effect of a change in the mechanical structure before the change is made. This would be most desirable because of the cost of even a minor change in such a large transducer. The facilities necessary for measurements on a large radiator are elaborate and it would thus be most helpful if scale modeling could be employed. This modeling of the rings was the main purpose of this work.

A complete set of small cylindrical Barium Titanate rings was fabricated through the efforts of Mr. T. Mapes of the Harris ASW Division of General Instruments Corporation. These rings were all made from similar cast cylinders so that the only variation from one ring to another was the length of the cylinder. The wall thickness of all of the rings was 1/8 inch, the outside diameter was 1-1/2 inches, and the lengths varied from 1/8 inch up to 1-1/2 inches. The height to diameter ratio turns out to be a most important design parameter and this ratio varies from 1:2 down to 1:1 in this ring set.

Only two of the set of nine rings were used in this study, and another pair of 1-inch outside diameter rings were used. Their lengths were 1/4 and 1/2 inches. The same measurements were made on all four of these model rings and these are presented in detail in the latter part of this report.

On of the serious questions here is the relative behavior of a single ring operating first in the pressure relieved configuration, and then

in the flooded arrangement. Using a small model ring this is simple to accomplish. A thin plastic membrane was cemented across each end of the ring. Radiation patterns and impedance curves were then recorded, after which, the membrane was removed from the ring. The experiments were immediately repeated without disturbing the ring in its support jig. This procedure produced the curve sets in the body of the report. The effect of flooding the inside of the ring is apparent in these curves.

The fundamental resonance frequency of the 1 - 1/2 inch diameter ring is about 40 Kcps. Since the deep-ocean rings are several feet in diameter, the model scale factor is the order of perhaps 50:1. The corresponding actual ring resonance would be about 800 cps. The water tank in which the measurements were made is 6 - feet in length or about 50 wavelengths. This is long enough to permit placing the receiver well removed from the radiator, but not long enough to avoid the necessity of making the measurements by means of short pulses. Even though the tank is lined with a highly absorbing material the reverberation level in the tank is such that gated transmitter and receiver setups are necessary.

The fundamental and higher-ordered circumferential resonance modes are related to each other in the same way in the model rings and in the full-scale rings. This is important because these modes as well as length modes and "squirter" modes cause the fluctuations

in response which are significant in the performance of the final radiator. Response curves and impedance curves serve well to identify the various resonance effects.

II

REVIEW OF THEORETICAL STUDIES OF RINGS

1. Model Radiator Extended by Two Semi-infinite, Rigid Cylindrical Baffles.

This model was first suggested by D. T. Laird and H. Cohen in 1952[2] and is believed to be the first attempt to solve the problem of radiation patterns of cylindrical transducers. It is an extended case of the problem of an infinite vibrating strip along the cylinder which has been solved by P. M. Morse[3]. The source in this theory can be any separable function of the azimuth and axial dimensions, e.g., a rectangular piston.

Using a cylindrical coordinate system with variables r, ϕ, z, Laird and Cohen gave the following expression for the boundary conditions at r = a where a is the radius of the cylinder:

$$u_r|_{r=a} = U_o e^{-i\omega t} \left(\sum_{m=o}^{\infty} a_m \cos m\phi \right) \left(\int_{-\infty}^{\infty} F(k_z)\, e^{ik_z z}\, dk_z \right)$$

where $u_r|_{r=a}$ is the source velocity distribution, U_o is the initial velocity condition, the a_m's are the Fourier coefficients determined by the source geometry, k_z is the wave number in the z-direction and $F(k_z)$ is the fourier transform of the velocity distribution in the z-direction. The Fourier series, which for simplicity has been taken to be a cosine series, gives the dependence on ϕ whereas the Fourier integral represents

the dependence on z.

The general solution of the wave equation in cylindrical coordinates is given by

$$p(r, \phi, z) = e^{-i\omega t}\sum_{m=0}^{\infty} \cos m\phi \int_{-\infty}^{\infty} A_m(k_z)\, H_m^{(1)}(k_r r) e^{ik_z z} dk_z$$

where p is the radiation pressure, $k_z^2 + k_r^2 = k^2 = \omega^2/c^2$, and $H_m^{(1)}$ is the first Hankel function of order m.

After matching this solution to the boundary conditions described above, introducing the wave zone approximation and replacing cylindrical coordinates by spherical coordinates represented by R, θ, ϕ, one obtains the final description of the radiation pressure:

$$p(R, \theta, \phi) = 2\rho c U_o \frac{e^{i(kR-\omega t)}}{R} \frac{F(k\cos\theta)}{\sin\theta} \sum_{m=0}^{\infty} \frac{a_m e^{-im\frac{\pi}{2}}}{H_m^{(1)'}(ka\sin\theta)} \cos m\theta$$

The approximations involved in this method can be argued to be just the usual wave zone approximation and the result obtained is a correct description of the wave zone field. This result can be applied to various source configurations, including a vibrating circular band on a rigid cylinder.[4] It can hardly, however, be applied to an isolated ring either flooded or air-backed by pressure-release caps where the velocity distribution at the end caps constitutes a not-insignificant part in vibration of the ring.

Another method of solving the same problem was given by D. H. Robey in 1954.[5] This method is more general and can well be

applied to an array of finite cylindrical sources which make up the active part of an infinitely long, rigid, cylindrical baffle.

The theory of the Green's Function for the Helmholtz Equation[6] is used here with inhomogeneous Neumann boundary conditions. Thus the normal gradient of the velocity potential resulting from the m^{th} source $\frac{\partial \phi_m(\vec{r}_o)}{\partial \nu_o}$ is non-zero which leads us to make the normal gradient of the Green's function zero at the surface:

$$\frac{\partial G(\vec{r}_o/\vec{r})}{\partial \nu_o} \Big|_s = 0$$

The velocity potential from the m^{th} source becomes

$$\phi_m(\vec{r}) = \int_s G(\vec{r}_o/\vec{r}) \frac{\partial \phi_m(\vec{r}_o)}{\partial \nu_o} dS_o$$

Now, the net potential resulting from the entire array is the summation of the individual rings:

$$\phi_a(\vec{r}) = \sum_m \phi_m(\vec{r})$$

If each source is assumed to vibrate with a constant amplitude, in phase everywhere over its surface, we can write

$$\frac{\partial \phi_a(\vec{r}_o)}{\partial \nu_o} = \begin{cases} -u_q e^{i\delta_q} & \text{over the } q^{th} \text{ source} \\ 0 & \text{over baffles} \end{cases}$$

and

$$\phi_a(\vec{r}) = -\sum_m u_m e^{-i\delta_m} \int_{s_m} G(\vec{r_o}/\vec{r})\, dS_o$$

The Green's Function for the infinite cylinder is obtained by the method given by C. H. Papas.[7] At the boundary, it becomes, in cylindrical coordinates:

$$G(r/a,\ z-z_o) = -\frac{1}{4\pi^2 a} \int_{-\infty}^{\infty} \frac{H_o^{(2)}(k_r r) e^{-ik_z(z-z_o)}}{k_r H_1^{(2)}(k_r a)}\, dk_z$$

where $H^{(2)}$ is the second Hankel function and a is the radius of the cylinder.

Thus the equation for the velocity potential is solved. From here, the radiation pressure and impedance can be obtained.

This method can also be used for the case of the liquid-filled squirting cylinder[8] mounted in the aperture of an infinite wall and various other boundary conditions. It is a very versatile method, but it still has the weakness of omitting the end effect of the cylinder, i.e., the circulation of the fluid around the edges of the cylinder.

In general, the model radiator extended by semi-infinite, cylindrical baffles can be applied to the free-flooded, finite cylinder only in the case when $ka \ll 1$, i.e., when the cylinder is acoustically transparent.

2. Method Using Series Of Spherical Wave Harmonics.

Due to the recent development of large and efficient digital computers, other methods have been developed to solve the cylindrical

radiator problem, making use of this new facility. One of these is by N. G. Parke III and W. Williams Jr.[9] in 1962.

Essentially, this method uses the same model as described above, i.e., the radiator with rigid end faces and pure radial harmonic vibratory motion of the cylindrical surface. With this sort of inhomogeneous Neumann boundary conditions, Parke and Williams derived an approximate solution using a series of spherical wave harmonics. This solution can be made as accurate as possible for certain boundary conditions by minimizing a "misfit integral" which is the error caused by approximating an infinite series by a finite series.

Briefly, the velocity potential can be written in spherical coordinates as:

$$\phi(r,\theta) = \sum_{n=o}^{\infty} a_n h_n^{(1)}(kr).P_n(\cos\theta) \quad , \quad n, \text{ even}$$

where $h_n^{(1)}(kr)$ is the spherical Hankel function of the first kind and P_n is the usual Legendre polynomial.

Applying the boundary conditions to find a_n, one obtains an infinite series of the form:

$$N(\theta) = \frac{\partial \phi(\theta)}{\partial n}\Big|_{\text{cylinder}} = \sum_{n=o}^{\infty} a_n \phi_n(\theta) \quad , \quad n, \text{ even}$$

Since the $\phi_n(\theta)$'s are not of the same set (they are not orthogonal), one cannot follow the usual procedure of determining the coefficients a_n as if they are of a general Fourier expansion. Instead,

one has to approximate the infinite series $N(\theta)$ by a finite series $G(\theta)$ of the form

$$G(\theta) = \sum_{n=o}^{N} a_n \phi_n(\theta)$$

and to minimize the error by minimizing the "misfit integral" E (or "variance") with respect to a_k:

$$\frac{\partial E}{\partial a_k} = \frac{\partial}{\partial a_k} \int_o^{\pi} [N(\theta) - G(\theta)]^2 \, W(\theta) \, d\theta = 0$$

where $W(\theta)$ is a suitably chosen weighting function or probability function of θ[10].

This brings us to a set of $\frac{N}{2} + 1$ equations with the even coefficients a_o, a_2, a_4,..., a_N as unknowns. Once the coefficients are obtained, the velocity potential $\phi(r,\theta)$ can be solved (all with the "must" help of a digital computer.)

An extended method of the same principle can be used to solve any arbitrary finite body of revolution by determining the distinct boundary regions for each. However, since the end caps must be rigid, it cannot apply to such problems as the free-flooded cylinder.

3. Finite-difference Method.

Much more extensive use of the digital computer is made by a new method (1963) designed to solve a large class of body shapes. This is the finite-difference method[11], based on a fundamental result of classical field theory and developed in matrix form suitable for coding in modern computers.

A thin elastic body (shell) of some configuration immersed in an infinite fluid medium is excited by a periodic force, or forces, $F_k e^{\omega t}$. The surface of the shell can be considered as composed of an array of m triangular surface elements or "rigid-pistons", i.e., each having a constant uniform velocity with constant phase angle. The source strength is constant on each triangle and is unknown. To find these source strength, a matrix equation must be solved. This matrix equation is obtained through a long process of reasoning making use of first the equality of the shell and fluid particle velocities at the base point of each piston and second, Fredholm's observation that an integral equation is the limiting form of a set of n linear algebraic equations in n unknowns.* The calculation of radiation pressure and velocity at a general field point, on or outside the surface, is done by mere substitution. For far fields, the calculations will be greatly simplified.

This method is exact within the assumptions or simplifications used in arriving at a particular model. From the viewpoint of practicality, this is a great advantage. However, a vast amount of computation must be done--for it to be exact--and re-done for every change of model configuration and of velocity distribution.

4. Variational Principle For Radiation Loading.

This method avoids the large-scale use of a digital computer and returns to the old method developed by Robey with some improvements in the mathematical model, making use of the classical variational principle.[12]

*See for example, O.D. Kellog, Foundations of Potential Theory, Dover Publications, Inc., New York, 1953, p. 287.

For the solid cylindrical radiator, rigid end caps are assumed but the circulation of the fluid around the edges of the radiator is allowed by an additional velocity distribution, $U\alpha(z)$, on the two semi-infinite cylinders. The radiation impedance then becomes:

$$Z = Z_r + Z_\alpha$$

where the impedance Z_α is associated with $\alpha(z)$ and is the correction factor to Robey's impedance. The Green's function for the Helmholtz equation, together with the inhomogeneous Neumann conditions, gives the following expression for the impedance Z_α:

$$Z_\alpha = i\omega\rho\ (4\pi a)^2\ J(\alpha)$$

where $J(\alpha)$ is a functional for the correct expression of $\alpha(z)$, i.e., that which satisfies the condition that the potentials be continuous across the cylinder boundary at $r = a$, $z > L$.

Junger went on to prove that $J(\alpha)$ is stationary with respect to first order variations $\delta\alpha$ about the correct function $\alpha(z)$. Using this result, a trial function $\alpha(z)$ which is chosen based on the energy balance consideration is used to find the functional $J(\alpha)$, and thus, Z_α.

For the open-ended, free-flooded cylindrical radiator of vanishing wall thickness, the outer potential, i.e., the potential outside the cylinder, is the same as the above case. The inner potential, however, differs from the solid case as to the range of integration and to the Green's function used. The continuity conditions at the boundary,

$r = a$ and $z > L$, being the same, the rest of the derivation follows much of the same pattern.

5. Iteration Technique For Cylindrical Radiator Problem.

Started early in 1963, this new method for solving the cylindrical radiator problem by R. S. Haas and F. H. Middleton[13,14] is coming to its final state of development. The method makes use of the simplicity of the spherical coordinates when applied to the radiation problem by approximating the short cylinder with a segment of the circumscribing sphere. It can well be extended to any source configuration that can be approximated by a segment of the circumscribing sphere and that has a symmetry about an axis.

The solution of such a problem is well known for a certain source velocity distribution. To find the correct distribution--that which satisfies all boundary conditions--, an iteration technique[15] is used.

The normal gradient of the pressure, $\sigma(\theta)$, has some specified value $\sigma_0(\theta)$ on S_1, the radiating segment, but is unknown on S_2, the rest of the sphere, where we only know that p (pressure and σ are continuous across the surface.

In order to start we assume some value for σ on S_2as well, such as $\sigma = o$. We then have σ specified on all of S and can compute a set of coefficients for the source distribution. If these coefficients were used from the start, however, they would not necessarily satisfy the boundary conditions on S_2, that is, the condition that p be continuous, or $p_{in} = p_{out}$.

To avoid this, we take a new value for p on S_2, the arithmetic

mean of p_{in} and p_{out} just obtained. Thus

$$p'_{in} = p'_{out} = \frac{p_{in} + p_{out}}{2}$$

This new value for pressure which satisfies the continuous condition on S_2 will probably not meet the boundary condition on S_1, that is, the condition that $\sigma_{in} = \sigma_{out}$.

Again, a new value for σ is obtained from the arithmetic mean of σ_{in} and σ_{out}:

$$\sigma'_{in} = \sigma'_{out} = \frac{\sigma_{in} + \sigma_{out}}{2}$$

This is an improved estimate of $\sigma(\theta)$. We are now ready to start over again from the beginning. The entire procedure can be repeated as many times as are necessary to get a good fit of both boundary conditions.

This method is attractive due to its simplicity and practicality. It can be easily coded for a digital computer. Its accuracy is great for $\frac{L}{D} \leq 1$, especially for far field potentials. It is also very versatile in view of the fact that it can be applied to different source configurations and many-segment problems.

III

RESULTS OF OTHER EXPERIMENTAL STUDIES

Only recently attempts[16,17] have been made to determine experimentally the characteristics of free-flooded cylindrical rings.

Up to a few years ago, the majority of Sonar transducers required some form of pressure-release for efficient operation. This pressure-release usually takes the form of either the specially developed materials such as "Corprene" and "Celltite" rubber or cavities inside the transducer filled with air. However, at depths in excess of 100 feet, "Corprene" and "Celltite" begin to fail due to loss of air from the cells of the material under hydrostatic pressure. This loss of air causes these materials to exhibit mechanical hysteresis effects under cyclic changes of pressure, and consequently, the acoustic properties of the transducers in which they are used are permanently impaired. The air-cavity systems can be made to operate efficiently down to much greater depths, limited only by the mechanical strength of the transducer. One can increase the maximum working depth of these systems by the use of compressed-air for pressure-compensation, but this requires additional bulky apparatus and if the system fails catastrophic failure of the transducer or array usually occurs. In view of these obvious disadvantages, deep-submergence transducers are often free-flooded or devoid of all forms of pressure-release. Because of their size and cost, there is considerable interest in learning about the behavior of such rings for convenience in

design.

In 1961, A.S. Merriweather used two sets of rings for an experiment. The first set consisted of rings of 1.5" in diameter and form 0.5" to 3.0" in length. The rings of the second set were 6.0" in diameter and 3.5" in length and were mounted either singly or doubly (forming a composite cylinder 7.0" in length.) The reason for using the second set was to check the validity of the scale modeling. The result was positive.

The experimental data in this work includes the admittance measurements in air, the impedance measurements in water, the receiving responses and the directivity patterns for each ring, both with and without "Celltite" as pressure-release material. Many conclusions can be drawn from these data, but they are limited to a rather short frequency range. It will be shown later that the length mode is considerably stronger at higher frequencies and can be used to great advantage.

In the years 1963 and 1964, General Instrument Corporation, Harris ASW Div. Westwood, Massachusetts, has done experimental work on free-flooded cylindrical transducers. Their models were 3", 5.25", 20.5" and 47.5" in diameter and of various length-to-diameter ratios, ranging from 0.167 to 0.6 for the 3" rings. There again, the validity of scale-modeling was verified. The results also showed that the percentage frequency reduction, i.e., the drop in circumferential mode resonant frequency when water-loaded compared to the air-loaded case, increases with increasing length-to-diameter ratio or decreasing thickness-to-diameter ratio. It was also found that the beam patterns remain essentially the same for the fundamental radial resonance. The limitations here are again in the short frequency range used. The knowledge on the radiation patterns as well as the efficiency of the rings is thus limited.

IV

RING DESIGN PARAMETER STUDY

In order to add to the present knowledge of cylindrical transducers, two pairs of rings were used in this study. The first pair was 1.5" in diameter, 0.125" in thickness, and 1.25" and 0.75" in height. The second pair was 1" in diameter, 0.125" in thickness, and 0.5" and 0.25" in height. [Dimensions before coating.] The reason for using two pairs, each with different heights was to isolate the effect of changes in the height-to-diameter ratio and the effect of changes in the radius of rings of the same thickness. It will be noted that all of these rings can well be fitted into the mathematical model of the theory by Haas and Middleton.[13]

The rings were connected by coaxial cables and coated with Neopreme N-11 primer followed by Neopreme N-29. Because of this extra mechanical load, the resonant frequencies are expected to drop slightly as well as the response on the end face that is partially clamped by the connecting cable.

The frequency range used in this study was from 10kc to 200kc. Due to the lack of a calibrated hydrophone adequate for this entire frequency range, the reciprocity method of calibration was used to obtain the absolute response of the transducers. The experimental results include impedance curves, response curves, radiation patterns and total power output at each mode, both in the flooded and air-backed arrangements. The air-

backed case was tested to observe the effect of pressure-release on the different modes of vibration of the rings. To obtain air-backing, two thin plastic membranes were glued to the ends of the rings. Due to this extra load plus the occasional air bubbles in the gluing material, the end response from the length mode is expected to drop.

1. Instrumentation.

[a] The Tank.

The model experiments were carried out in a rectangular tank 75 cm wide, 190 cm long and 75 cm deep. The tank was anechoic at the high end of the frequency range [10 kc-200 kc] because of a lining of wedge-shaped foam rubber. To obtain good results over the entire frequency range, the pulse technique was necessary.

To get the best out of the small dimensions of the tank, the transducers are placed near the center, 50 cm apart. At this distance, the sound wave-front can be considered plane and the sound field far for the lowest frequency used. [At 20 kc, the wave length is about 7.5 cm]. At this distance also, the transmit pulse will take 0.34 msec to reach the receiver by the direct path and 0.54 msec by the shortest reflected path. This allows a maximum pulse width of 0.2 msec which is quite adequate since it contains four cycles of a 20 kc signal. Due to reverberation, the masimum allowable pulse repetition rate is 60 pulses per second as can be seen on the oscilloscope.

[b] The Driving Mechanism.

The ring was rotated synchronously with the polar paper so that its radiation patterns could be plotted with accuracy. This was

done by taking advantage of the output drive shaft II of the B and K level recorder type 2305. A flexible cable is used with this drive shaft to drive the transducer through a special gearing system at speeds varying from .75 rpm down to a very slow speed. To minimize the position error caused by the flexible cable, the total gear ratio of the gearing system is chosen to be 160:1.

To complete the mechanical instrumentation, another flexible cable is used in connection with the output drive shaft I of the recorder to drive the variable capacitor of the B and K beat frequency oscillator type 1013 and the relative response of the transducer is plotted on frequency calibrated paper. Holding the ring in place during rotation underwater also presents a problem since clamps are very likely to hamper the vibrational motion of the ring. An adequate clamp was finally designed. Figure 1 is a block diagram of the complete mechanism.

[c] Electronic Equipment.

The pulse technique was used with the aid of the following standard electronic equipment:

Beat Frequency Oscillator, Bruel and Kjaer Type 1013

Level Recorder, Bruel and Kjaer Type 2305

Electronic Counter, Hewlett Packard, Model 523 DR

Receiver Gate, Scientific Atlanta, Type 1112

Transmitter Gate, Scientific Atlanta, Type 1111

Power Supplies, Harrison Laboratories, Model 6204 A

Pulse Generator, Rutherford Electronics Co., Model B-2 A

Pulse, Sweep and Time Delay Generator, General Radio, Type 1391-B

Square Wave Generator, Hewlett Packard, Model 211A

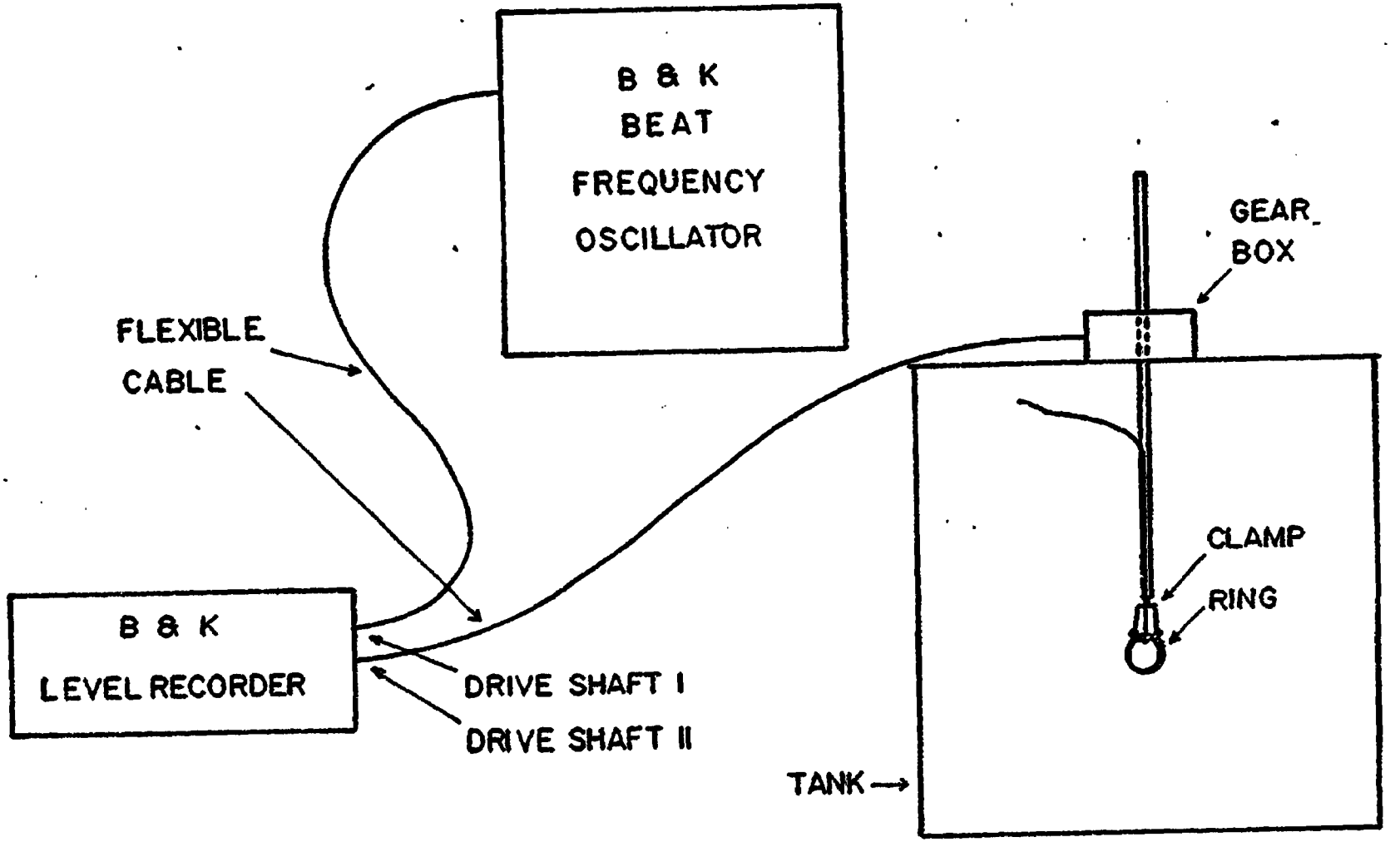

FIG 1 BLOCK DIAGRAM OF DRIVING MECHANISM

AC Amplifier [2], Hewlett Packard, Model 466A

Oscilloscope, Hewlett Packard, Model 175A

Besides this standard equipment, a specially designed transmitter gate was used. It has some desirable characteristics which will be discussed later in this section.

The R.F. signal was generated with great stability by the B and K beat frequency oscillator. Its frequency was accurately determined by the Hewlett Packard electronic counter. The oscillator was gated by pulses from the General Radio Pulse Generator in the transmitter gate and then fed directly to the transducer.

As the frequency changes, the electrical impedance of the transducer changes also, tremendously at resonances. In order to calibrate the transducer, the driving voltage must stay constant. But the driving voltage at the transducer is in the form of pulses--it has been gated--and cannot be fed back to regulate the output of the beat frequency oscillator. Thus the feed-back signal must be taken out before the transmitter gate. In addition, the signal level before and after the gate has to be approximately the same so that no amplification is necessary in the feedback loop. All these requirements are fulfilled in the transmitter gate shown in Figure 2. The 20 ohm resistor is used for better cutoff and for measuring the current in the transmitting transducer for calibration purposes. The voltage drop across it is considered negligible.

Thus the gated signal of constant voltage is fed to the transducer in the water. The acoustic signal is received by a hydrophone, amplified 20 db, and fed to the Scientific Atlanta receiver gate. The

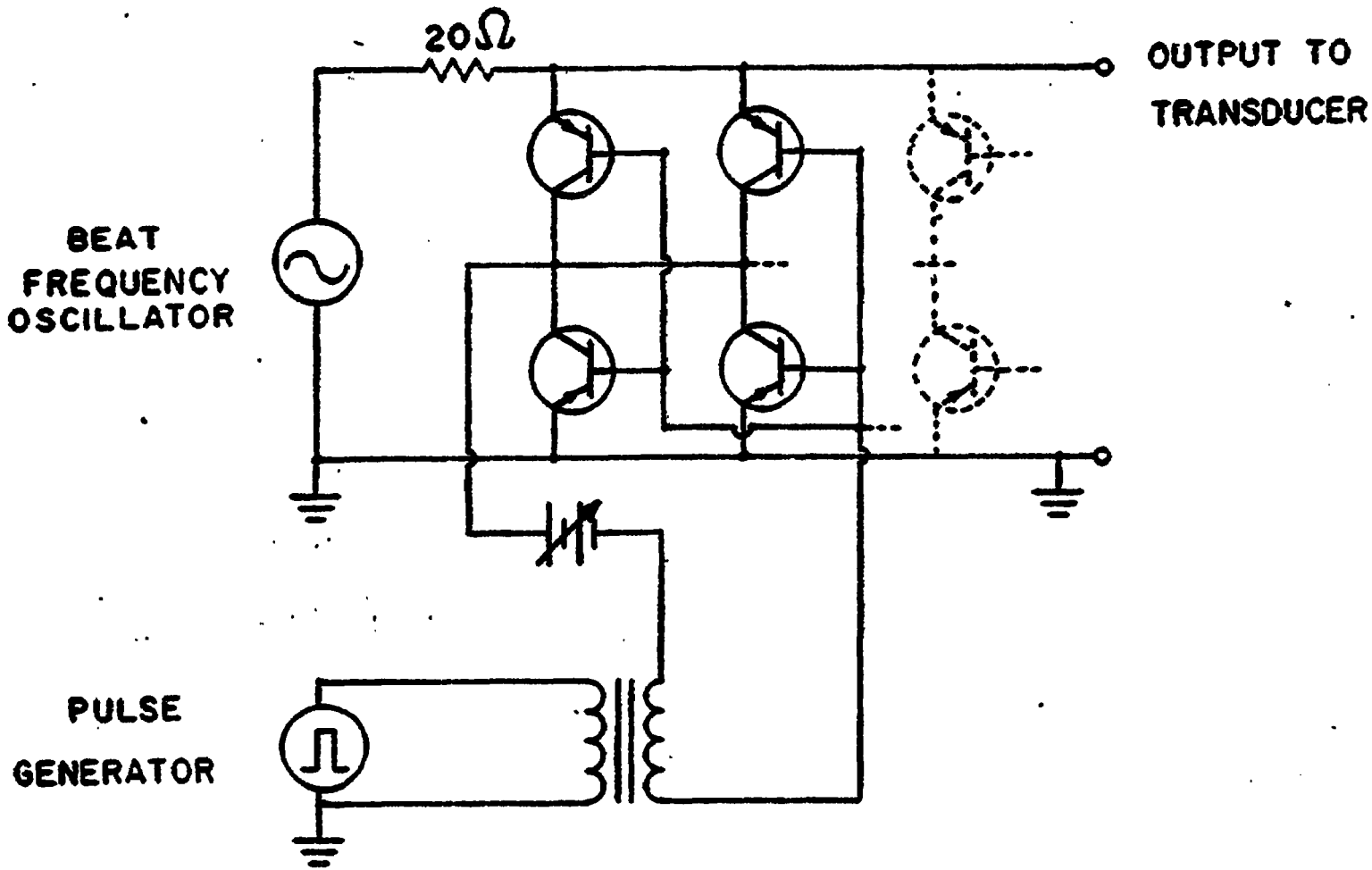

FIG 2 DIAGRAM OF TRANSMITTER GATE

pulses triggering the receiver gate are provided by the Rutherford Generator and delayed by 0.34 msec compared to the transmit pulses. A Hewlett Packard square wave generator is used to trigger both pulse generators externally. The purpose of this is two-fold: the generators are automatically synchronized and a very low pulse repetition rate is obtained.

Finally, the gated signal is amplified another 40 db before being recorded by the B and K level recorder. Figure 3 is a block diagram of the electronics arrangement.

2. Absolute Calibration Of Transducers.

As mentioned above, because of the lack of a calibrated hydrophone workable in the entire frequency range used, the reciprocity method of calibration was used to determine the response of two of the four transducers.

The reciprocity principle was first stated by Lord Rayleigh and can be expressed as follows, in acoustical terms: "Let an enclosed region have bounding surfaces s_1, s_2, s_3, ... , and let two separate distributions, generally different, of normal velocities v' and v" over the bounding surfaces produce pressure fields p' and p", respectively, over these surfaces. Then the surface integral of [p"v' - p'v"] over all the bounding surfaces s_1, s_2, s_3, ... vanishes."[18]

When the region considered contains only one simple source, the general reciprocity theorem may be reduced to a form ascribed to Helmholtz, i.e., "In a region partially bounded and partially unbounded, a simple source at any point A produces the same sound pressure at

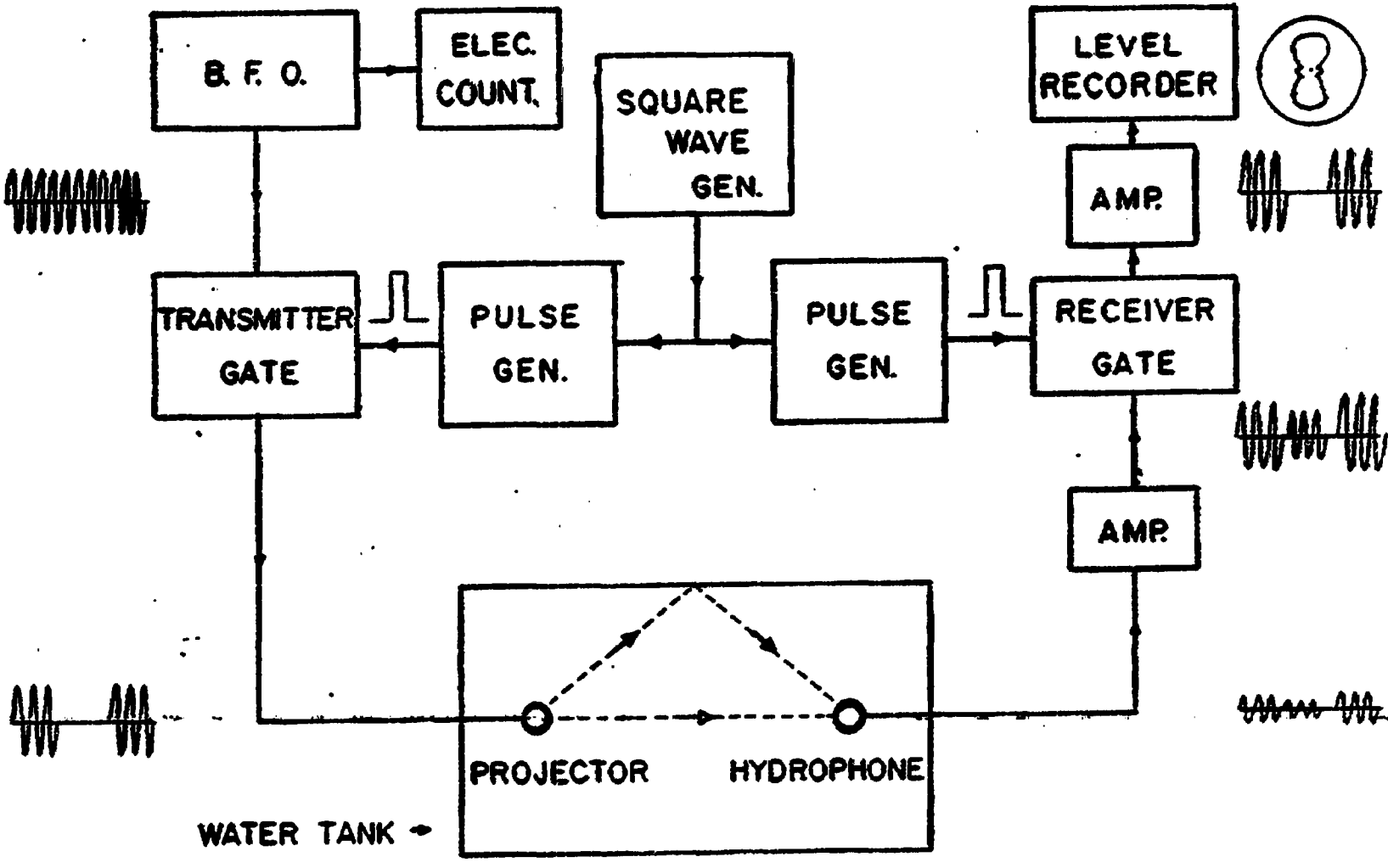

FIG 3 BLOCK DIAGRAM OF ELECTRONICS ARRANGEMENT

another point B as would have been produced at A had the source been located at B." This statement when applied to electroacoustics can be restated in the form, "If a simple source of strength Q_1 at a point A produces a sound pressure P_2 at a point B, then a simple source of strength Q_2 at B will produce a sound pressure P_1 at A such that

$$\frac{Q_1}{P_2} = \frac{Q_2}{P_1}"^{18} .$$

In this form, the theorem is analogous to the familiar reciprocity theorem for linear passive electrical networks. From the equivalent circuit of an electroacoustic transducer, one can prove that the ratio of the freefield receiving response, R, to the transmitting response, T, of a transducer is a constant J, called the reciprocity constant, depending only on the frequency, the medium and the distance between A and B:

$$\frac{R}{T} = J = \frac{2d}{f\rho_o}$$

In order to apply this result to the calibration of transducers, three sets of measurements must be made with three transducers, one of which must be reversible, a condition satisfied by all piezoelectric transducers.[19] It has been found advantageous to calibrate absolutely all four transducers with just four sets of measurement--a distinct advantage over calibrating one transducer with three sets of measurements. Thus the four transducers A, B, C, and D are calibrated by measuring the current in the transmitter and the voltage at the receiver at different

frequencies in each of the four arrangements below:

	Current	Transmitter	Receiver	Voltage
[1]	I_A	A	B	E_B
[2]	I_A	A	C	E_C
[3]	I_A	A	D	E_D
[4]	I_C	C	B	E_B'

and using the following formulae* for calculating the receiving and transmitting response of each:

$$R_A = \left(\frac{E_B \, E_C \, I_C}{E_B' \, I_A^2} J \right)^{\frac{1}{2}}$$

$$T_A = \frac{R_A}{J}$$

$$R_B = \left(\frac{E_B' \, E_B}{E_C \, I_C} J \right)^{\frac{1}{2}}$$

$$T_B = \frac{R_B}{J}$$

$$R_C = \frac{R_B \, E_C}{E_B}$$

$$T_C = \frac{R_C}{J}$$

$$R_D = \frac{R_B \, E_D}{E_B}$$

$$T_D = \frac{R_D}{J}$$

*A partial proof of these can be found in Kinsler and Frey, Fundamentals of Acoustics, 2nd Ed., Wiley page 328, -329. The rest can easily be deduced.

In the MKS system of units, R is expressed in volts per newton/m^2 and T is in newton/m^2 per ampere. To convert the transmitting response into newton/m^2 per volt which is a more useful form, T is divided by the electrical impedance Z of the transducer at each frequency.

One can avoid most of the data taking and calculations involved in this method of recording the transfer characteristics of the system, i.e., the output voltage of the receiver as the frequency range is scanned and the input current is kept constant for each of the arrangements 1, 2 and 4. Since a logarithmic scale is used, the transfer characteristics of the system from A to B (curve No. 1) is the summation of the transmitting response of A, T_A, and the receiving response of B, R_B:

$$T_A + R_B$$

Similarly, curve No. 2 of the system A to C is:

$$T_A + R_C$$

and curve No. 3 of the system C to B is:

$$T_C + R_B$$

Subtracting curve No. 1 from curve No. 2, one has:

$$(T_A + R_C) - (T_A + R_B) = R_C - R_B$$

Adding this curve to curve No. 3, one has:

$$(R_C - R_B) + (T_C + R_B) = T_C + R_C$$

This new curve is the summation of the transmitting and receiving responses of a reversible transducer. These responses are related by the factor J, the reciprocity constant. Now, since $J = \frac{2d}{f\rho_o}$ is inversely proportional to the frequency, on a logarithmic scale it will decrease 6 db per octave. This means that, ignoring scales, the transmitting response of the transducer with its driving current constant will differ from its receiving response by an increase of 6 db per octave.

Using this result, one can obtain an unscaled receiving response curve for the transducer by substracting 6 db per octave from the last curve obtained above and then dividing the resulting curve by two, using any arbitrary base-line.

Finally, the curve can be put into proper absolute scale if the true magnitude of one point is known. This requires only one reciprocity calculation for one particular frequency.

Knowing the receiving response, the transmitting response of any transducer can be obtained by simply subtracting this from the transfer characteristics of the system with either constant driving current or voltage. The proper scale can be found either by knowing the absolute magnitude of one point [reciprocity method] or by using the proportionality relationship between the pressure produced at the receiver and its output voltage at one particular frequency. Once the scale factor for one transmitter is known, it can well be used for others as long as the driving voltages or currents are the same.

3. Experimental Procedure.

One must first make sure that the transmitting pulses are

clean and even and that the receiving pulses are free of reverberation interference. These conditions are satisfied as can be seen in Figure 4 and Figure 5 for two typical resonant frequencies. Questions might arise as to the shape of the directly received pulses, but this is due to transient at resonance which, however, has no effect in the results since a peak-to-peak rectifier response is used for the recorder. The pulse repetition rate is 60 pps and the driving voltage is constant at 10 volts peak-to-peak. Note in Figure 4d that the direct electrical pick-up has disappeared due to the air-backing membranes.

Before proceeding with the calibration, the driving point impedance curves of the four transducers were plotted. This was done automatically by the B and K level recorder, plotting the voltage across the transducer for a constant driving current. The current is kept constant by feeding back to the compressor input of the B and K beat frequency oscillator a sufficiently large voltage across a resistor in series with the transducer. See Figure 6 for the circuit diagram.

Two sets of curves are plotted, one for the air-loaded and the other for the water-loaded case. These are shown in Figures 7a-d.

The pulse calibration is then carried out, using the second method as described above. The transfer characteristic curves of different arrangements of transducers are plotted by the B and K level recorder. See Figures 8a-d. For each transducer that is used as the projector, both the cylindrical and acoustical axes are tested in the free-flooded as well as the air-backed case. The receiver, B or C, is always free-flooded with the acoustical axis facing the projector.

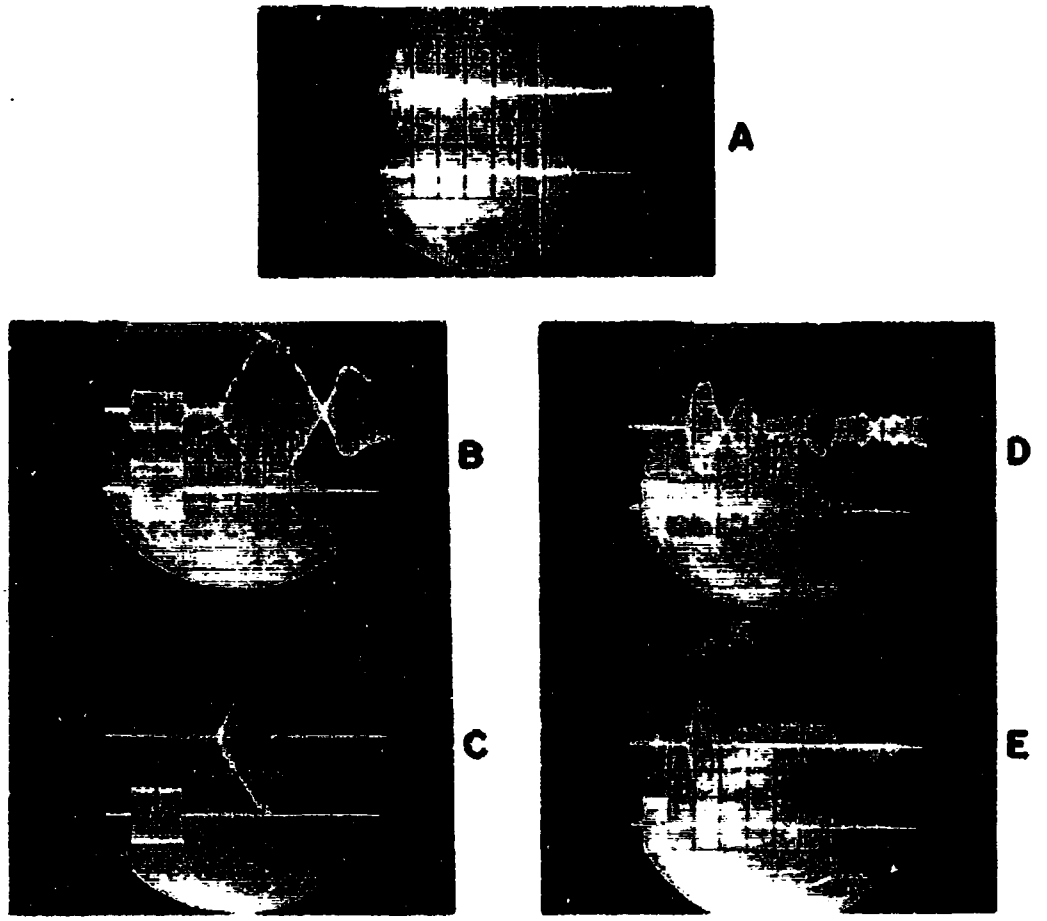

FIG. 4 CRT PHOTOGRAPH OF 37 KC SIGNAL

A = Complete Transmitted and Received Signals

B & C = Flooded Case, Non-gated and Gated

D & E = Air-backed Case, Non-gated and Gated

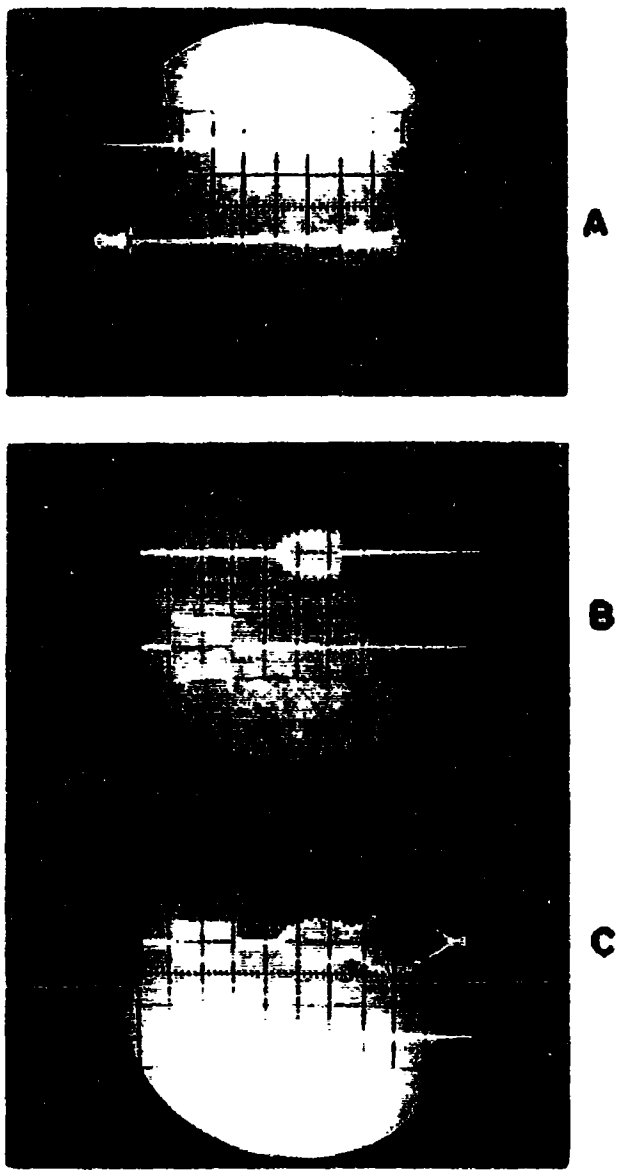

FIG. 5 CRT PHOTOGRAPH OF 74 KC SIGNAL

A = Complete Transmitted and Received Signals

B & C = Flooded Case, Gated and Non - gated

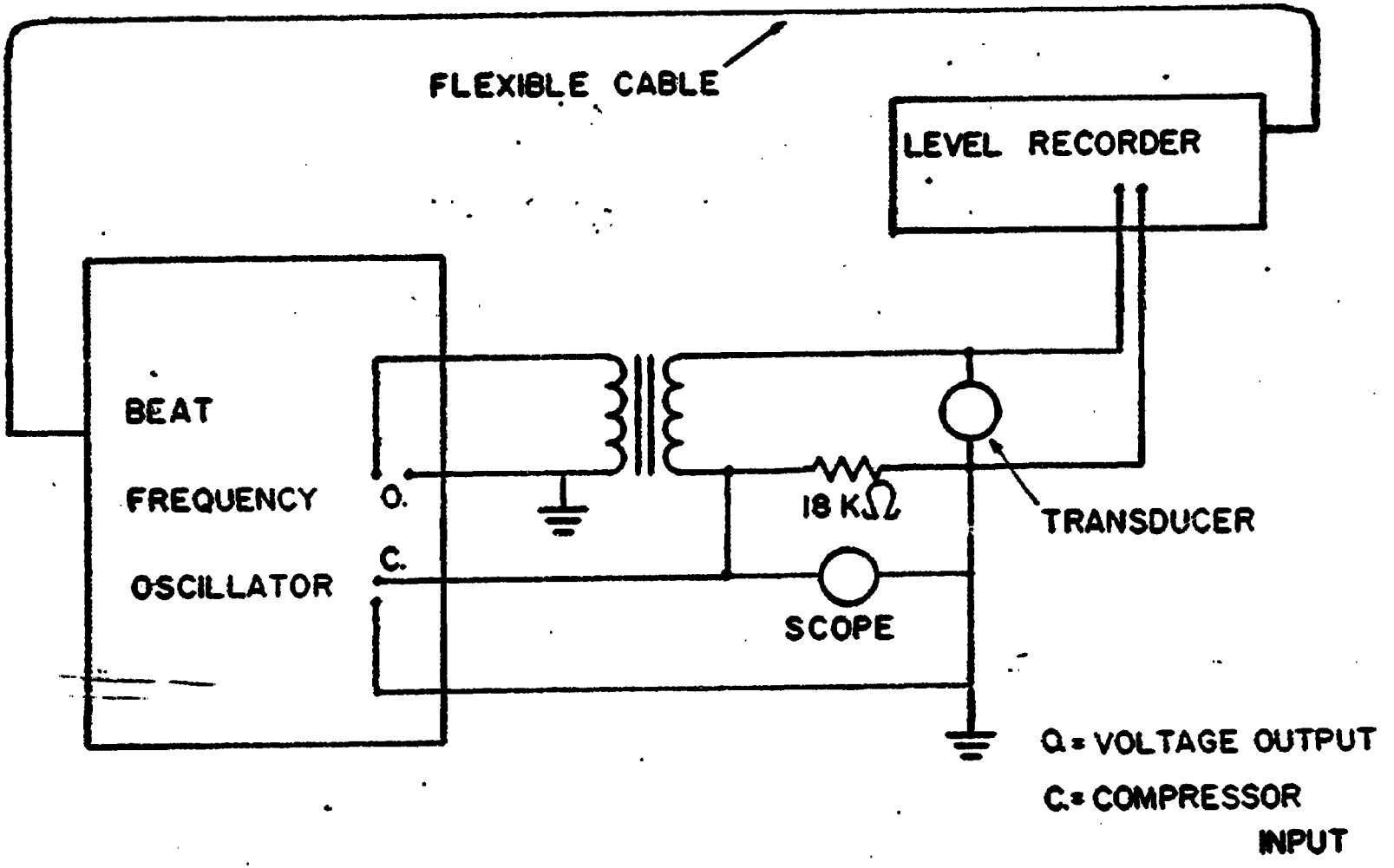

FIG. 6 CIRCUIT DIAGRAM FOR TRANSDUCERS' IMPEDANCE PLOTTING

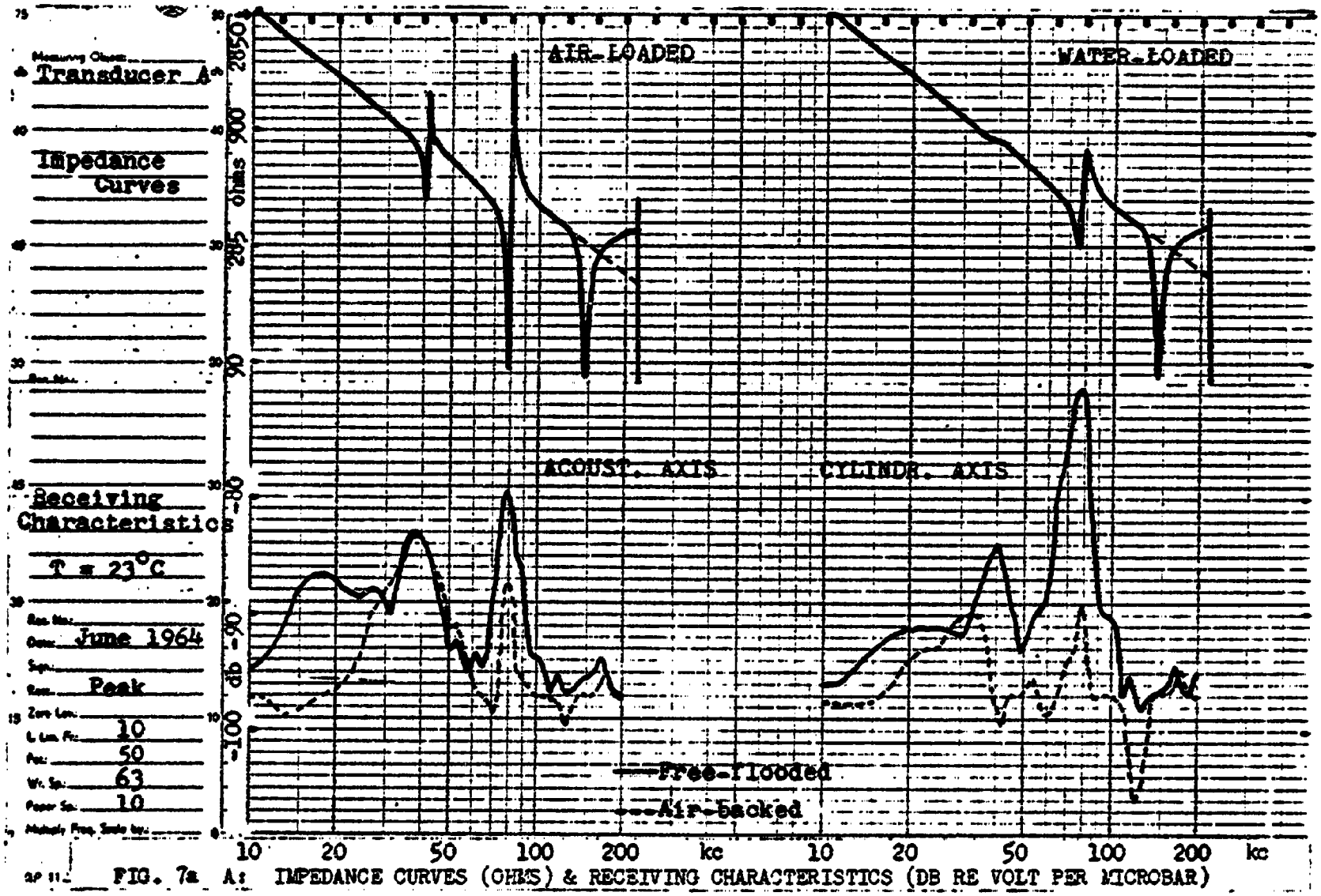

FIG. 7a A: IMPEDANCE CURVES (OHMS) & RECEIVING CHARACTERISTICS (DB RE VOLT PER MICROBAR)

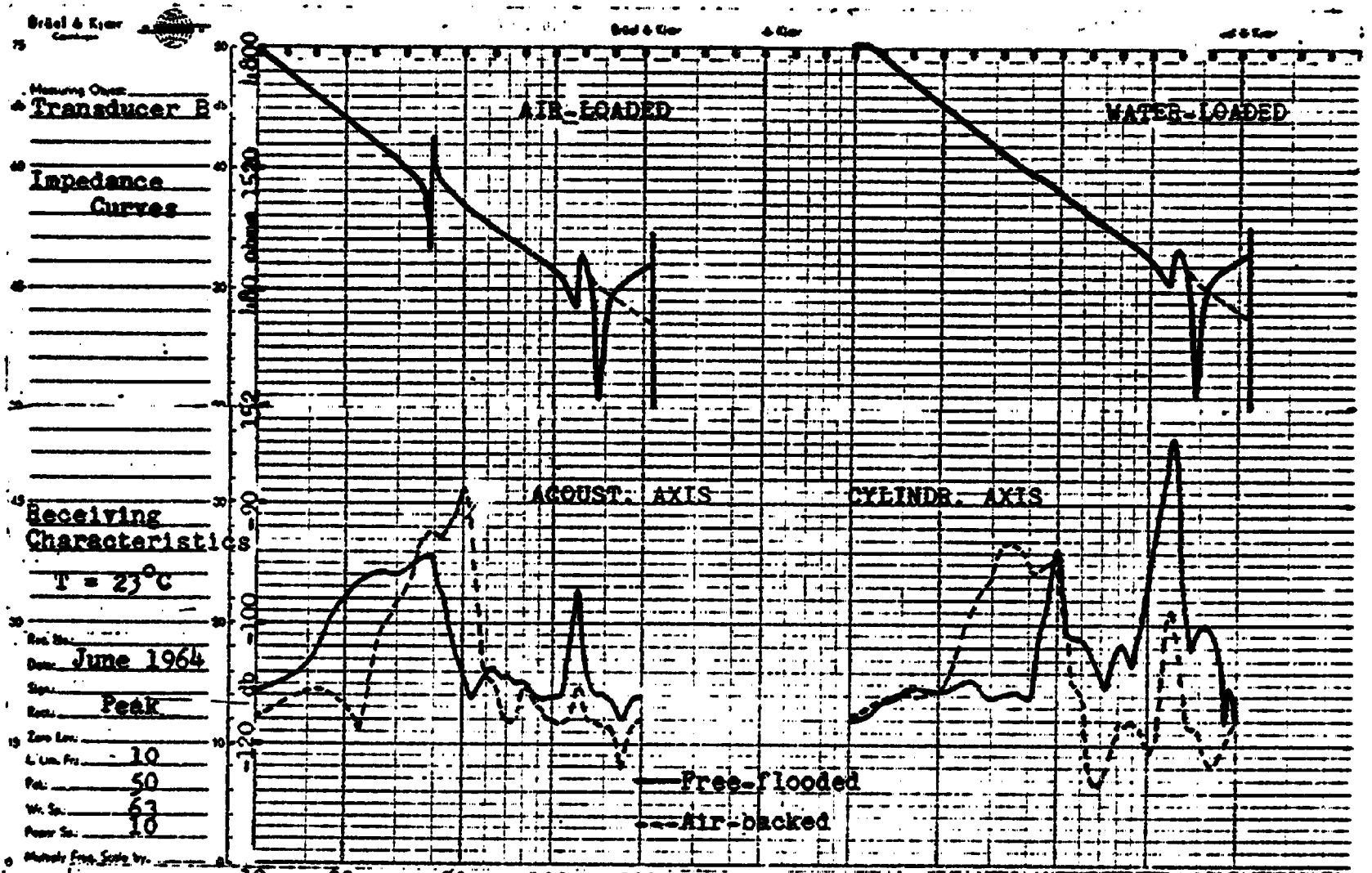

FIG. 7b B: IMPEDANCE CURVES (OHMS) & RECEIVING CHARACTERISTICS (DB RE VOLT PER MICROBAR)

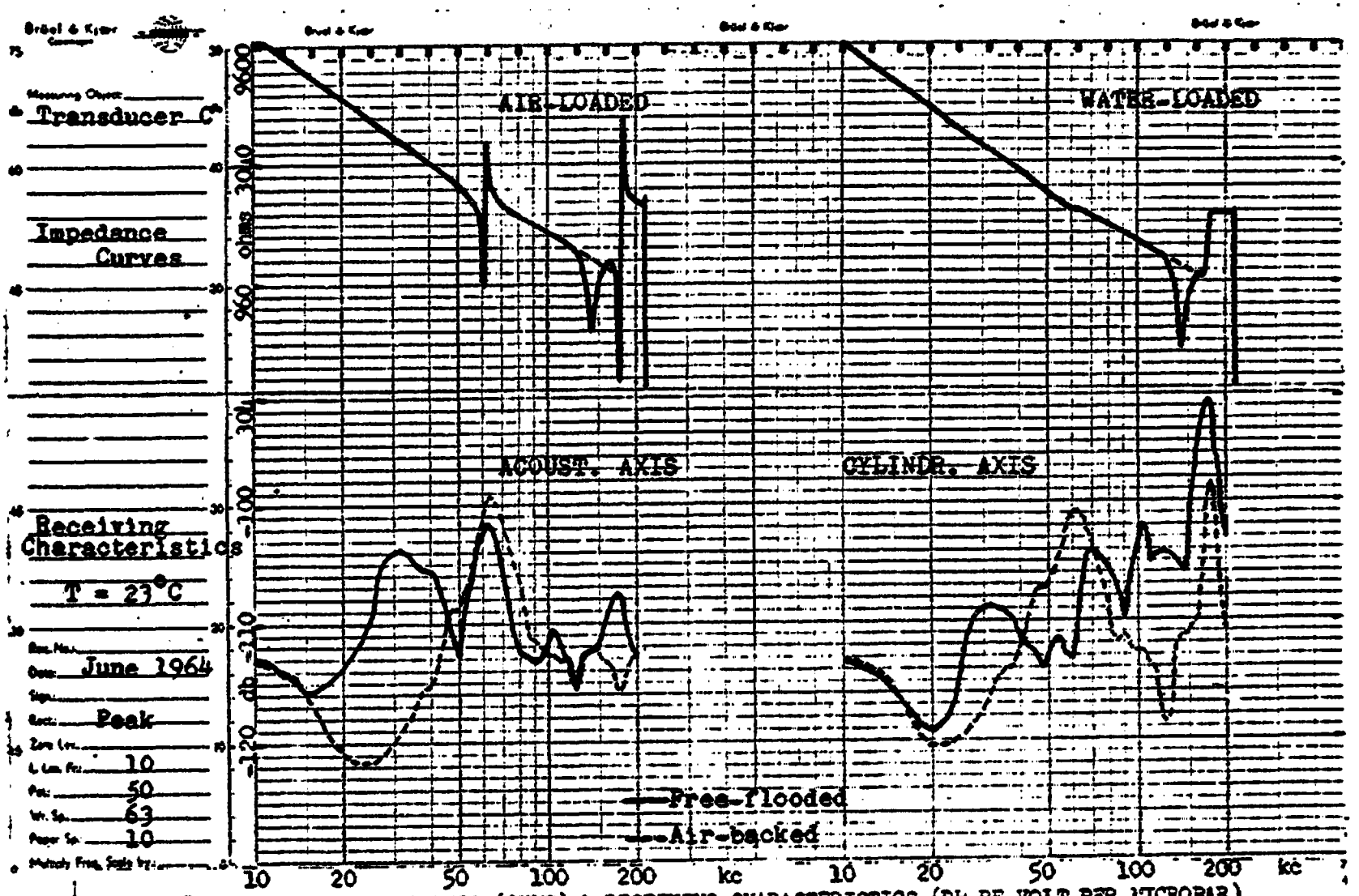

FIG. 7c C: IMPEDANCE CURVES (OHMS) & RECEIVING CHARACTERISTICS (DB RE VOLT PER MICROBAR)

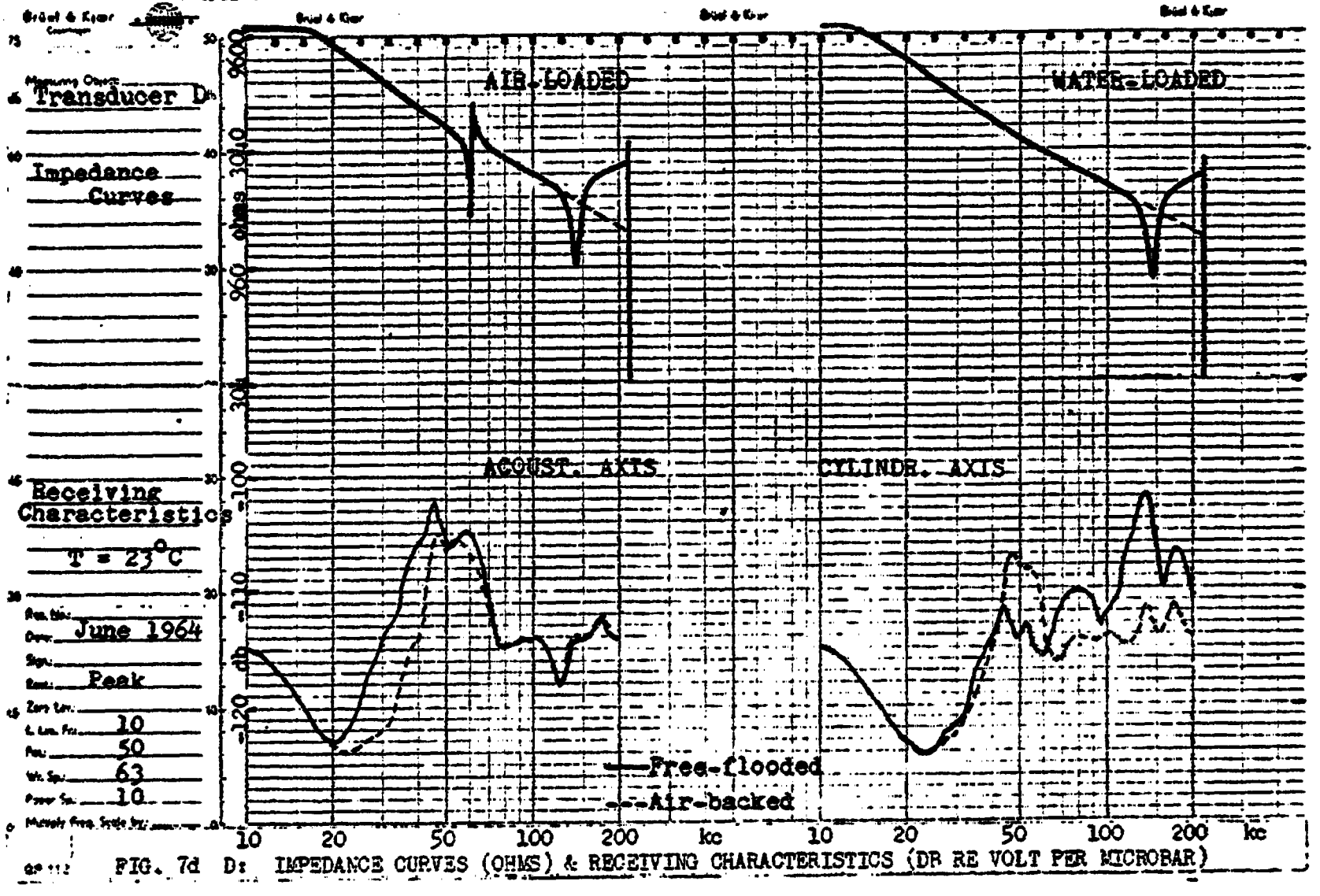

FIG. 7d D: IMPEDANCE CURVES (OHMS) & RECEIVING CHARACTERISTICS (DB RE VOLT PER MICROBAR)

The receiving response of B, acoustical axis, is obtained first. Subsequently, the receiving response of all the transducers are obtained by simple subtraction of curves. The reciprocity calibration method is used for one frequency, 37 kc, for the absolute magnitude of one point of each of the curves. This frequency is chosen to eliminate the error due to the inevitable imperfection in aligning the two acoustical axes of the two rings. It is known that at this frequency, the beam patterns for all the four rings are very broad and even on the acoustical axis, a result to be seen later when the radiation patterns are plotted.

Since it is the transmitting response per volt in that is of interest, for simplicity of the arithmetic, the receiving characteristics are not corrected by the 6 db per octave difference between volts per microbar - per ampere, nor are they corrected by the difference between microbar per ampere and microbar per volt (the electrical impedance factor). The absolute response at 37 kc being known, to get that at 74 kc, an octave higher for example, one simply has to subtract 3 db plus the difference (in db) between the water-loaded impedances at 37 kc and at 74 kc. These so-called receiving characteristic curves are shown in Figures 7 a-d together with the impedance curves for convenience.

The transmitting response of the transducers are needed only at frequencies where the total power output is to be computed. They are plotted in Figure 9 a-b.

The next step is to plot the radiation patterns of the transducers at different frequencies. This is done on polar paper by the B and K level recorder with the help of the gearing system described above.

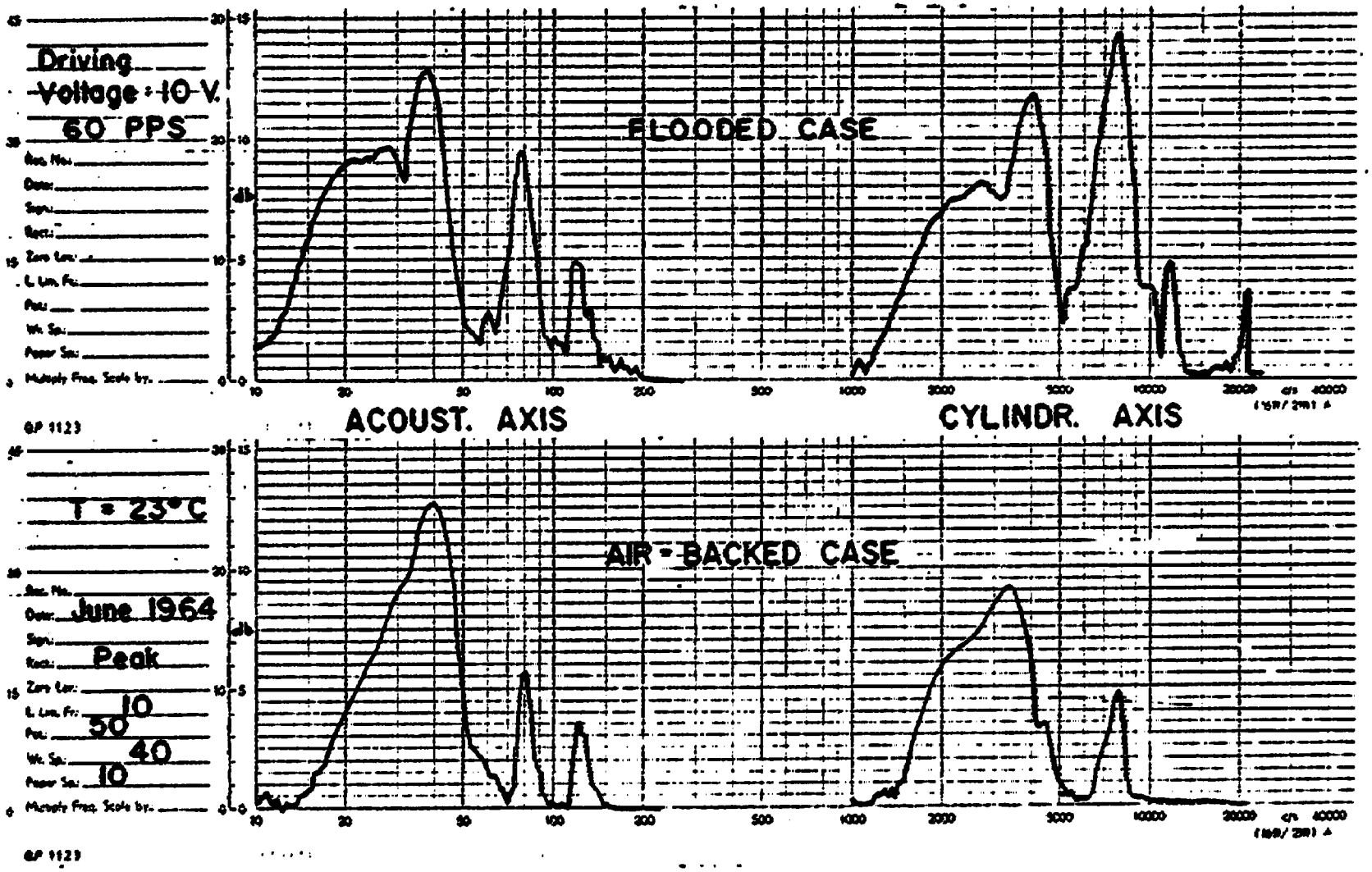

FIG. 8a TRANSFER CHARACTERISTICS OF A - B SYSTEM

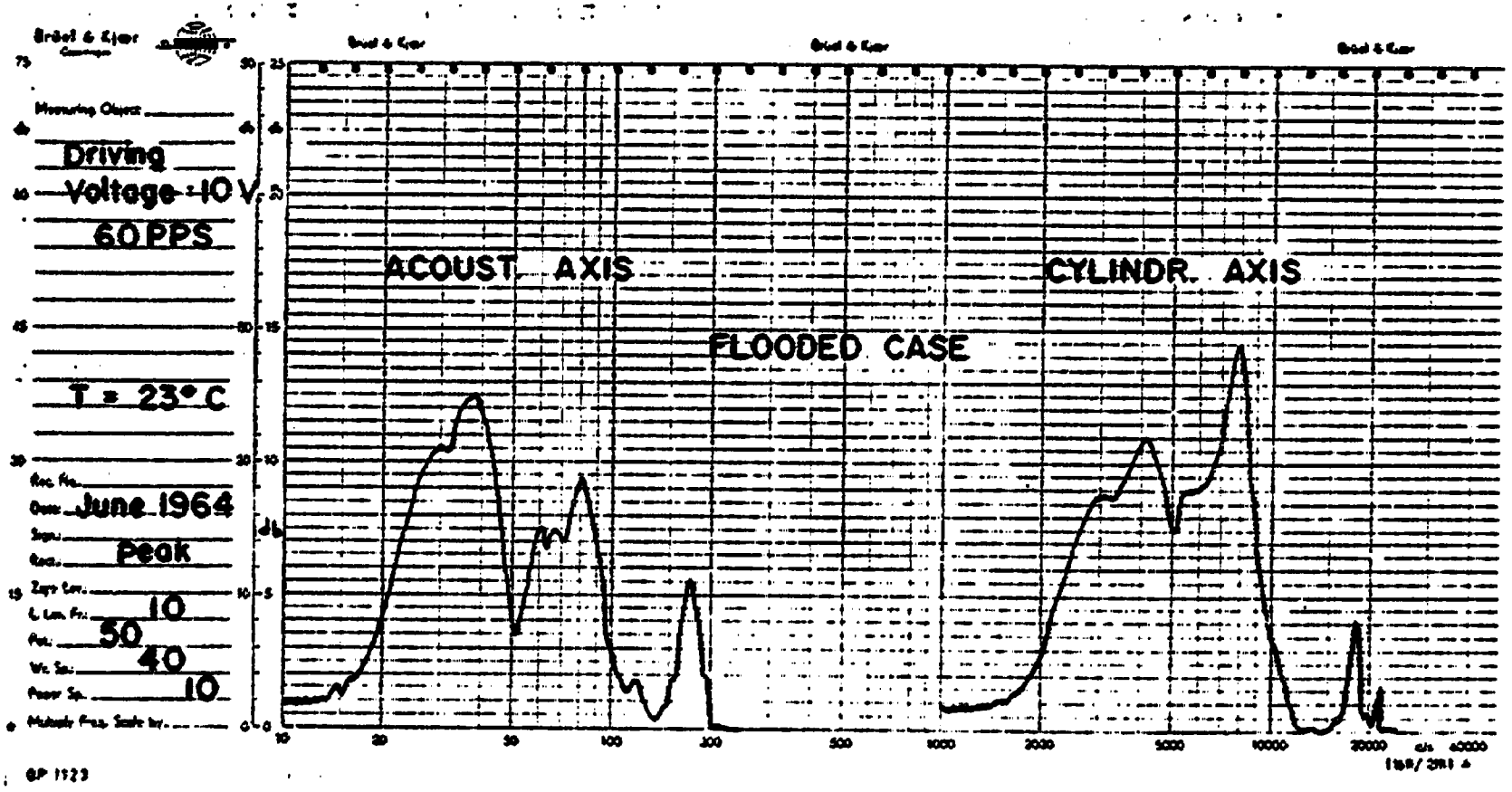

FIG. 8a' TRANSFER CHARACTERISTICS OF A-C SYSTEM

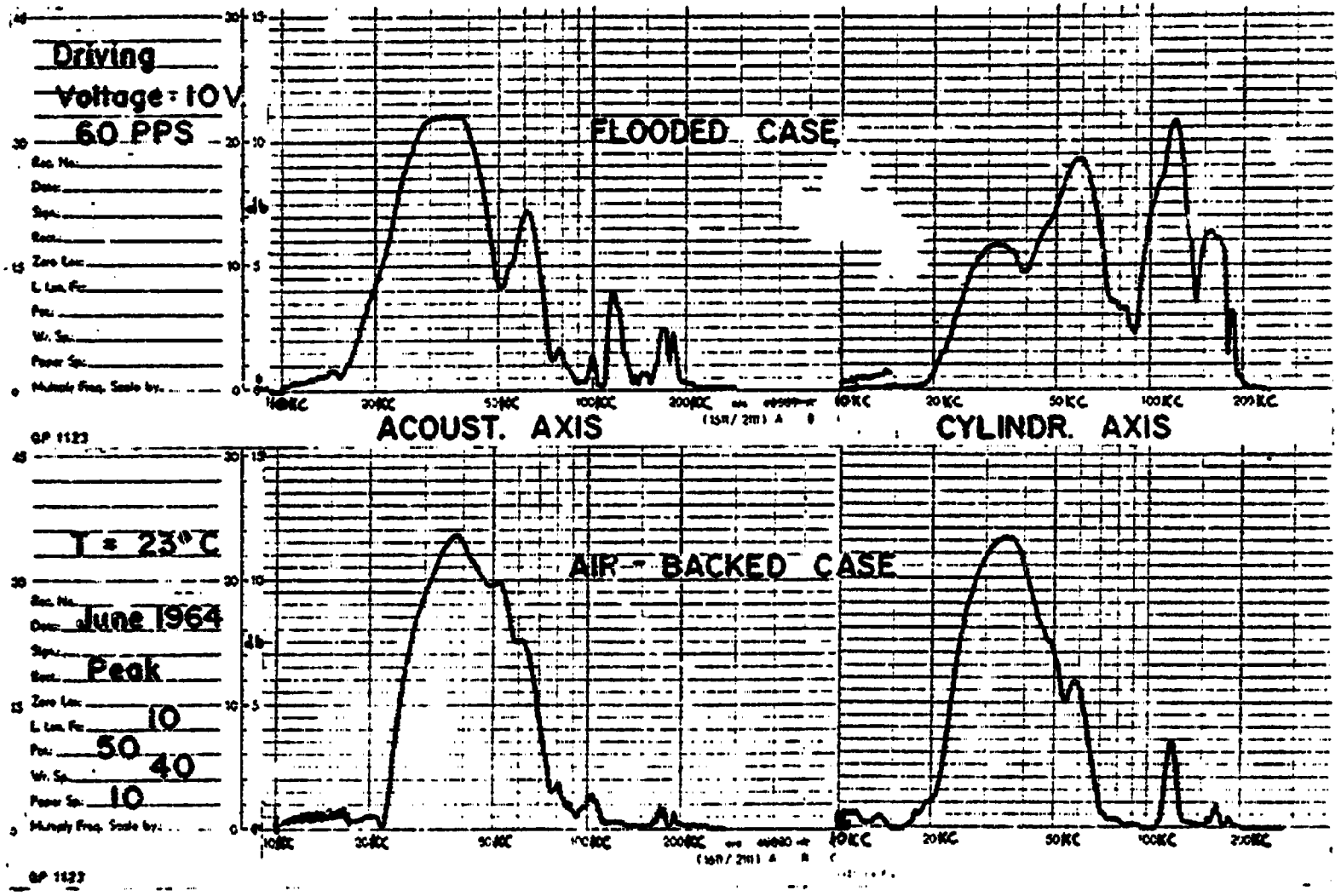

FIG. 8b TRANSFER CHARACTERISTICS OF B-C SYSTEM

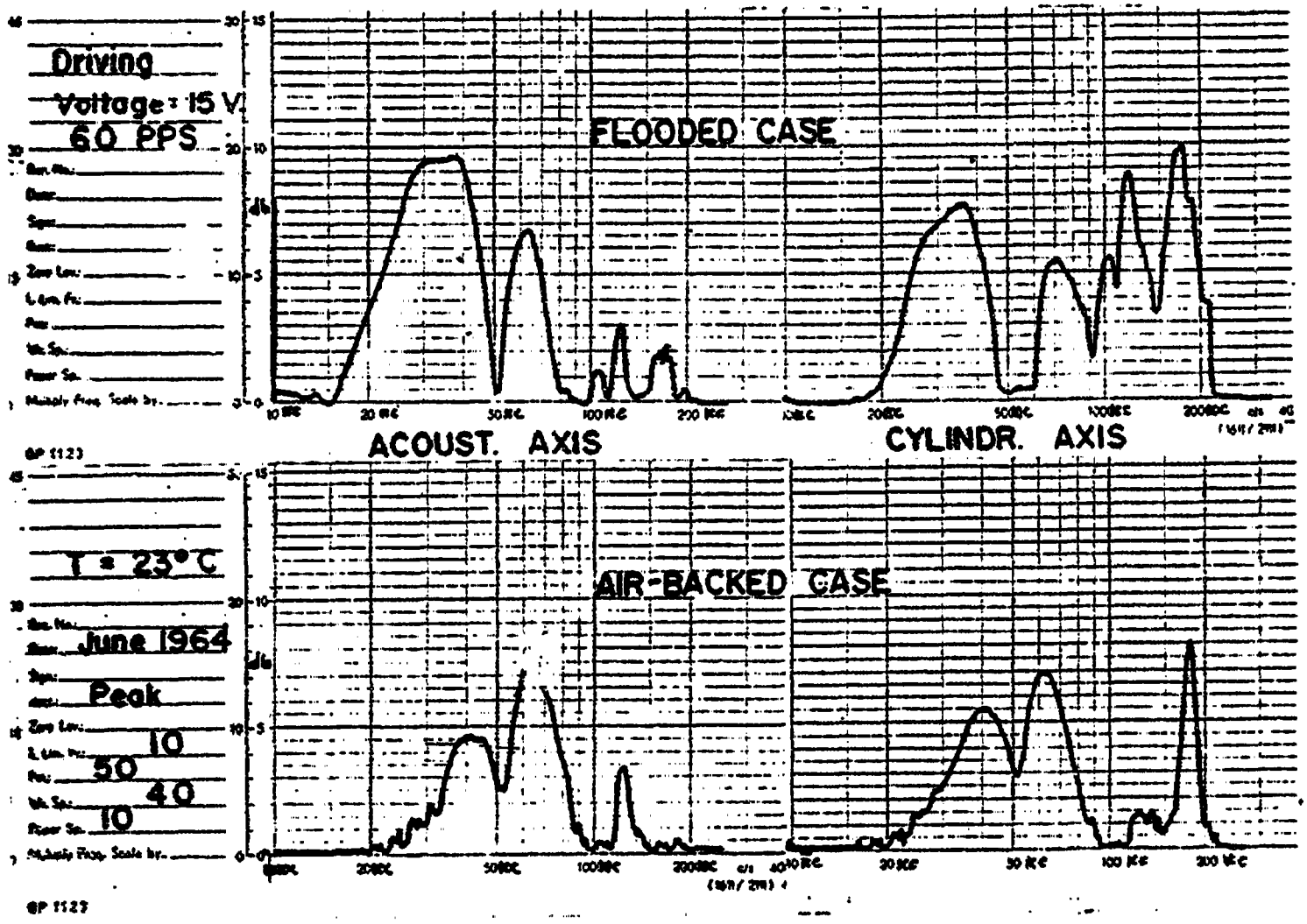

FIG. 8c TRANSFER CHARACTERISTICS OF C-B SYSTEM

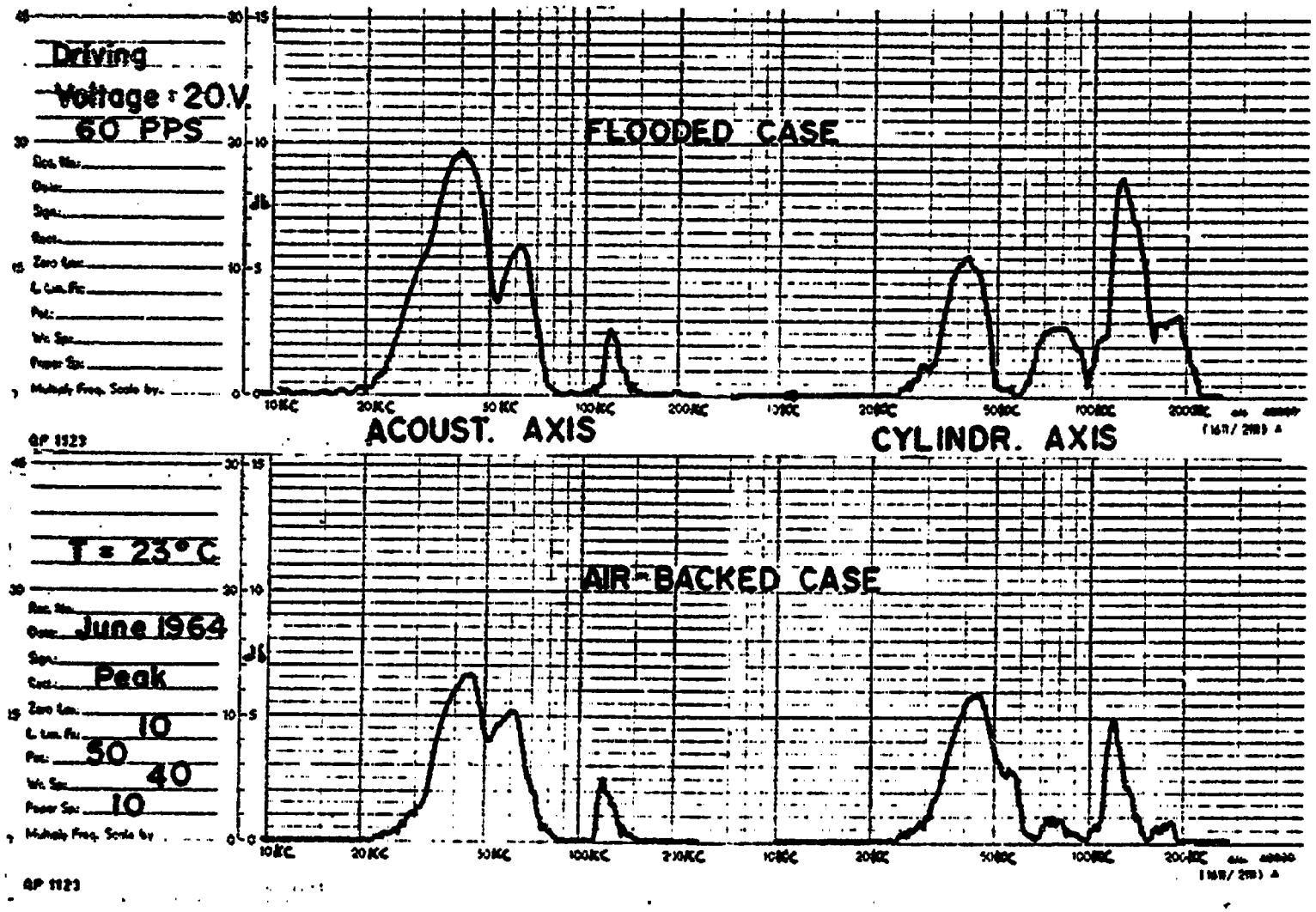

FIG. 8d TRANSFER CHARACTERISTICS OF D-B SYSTEM

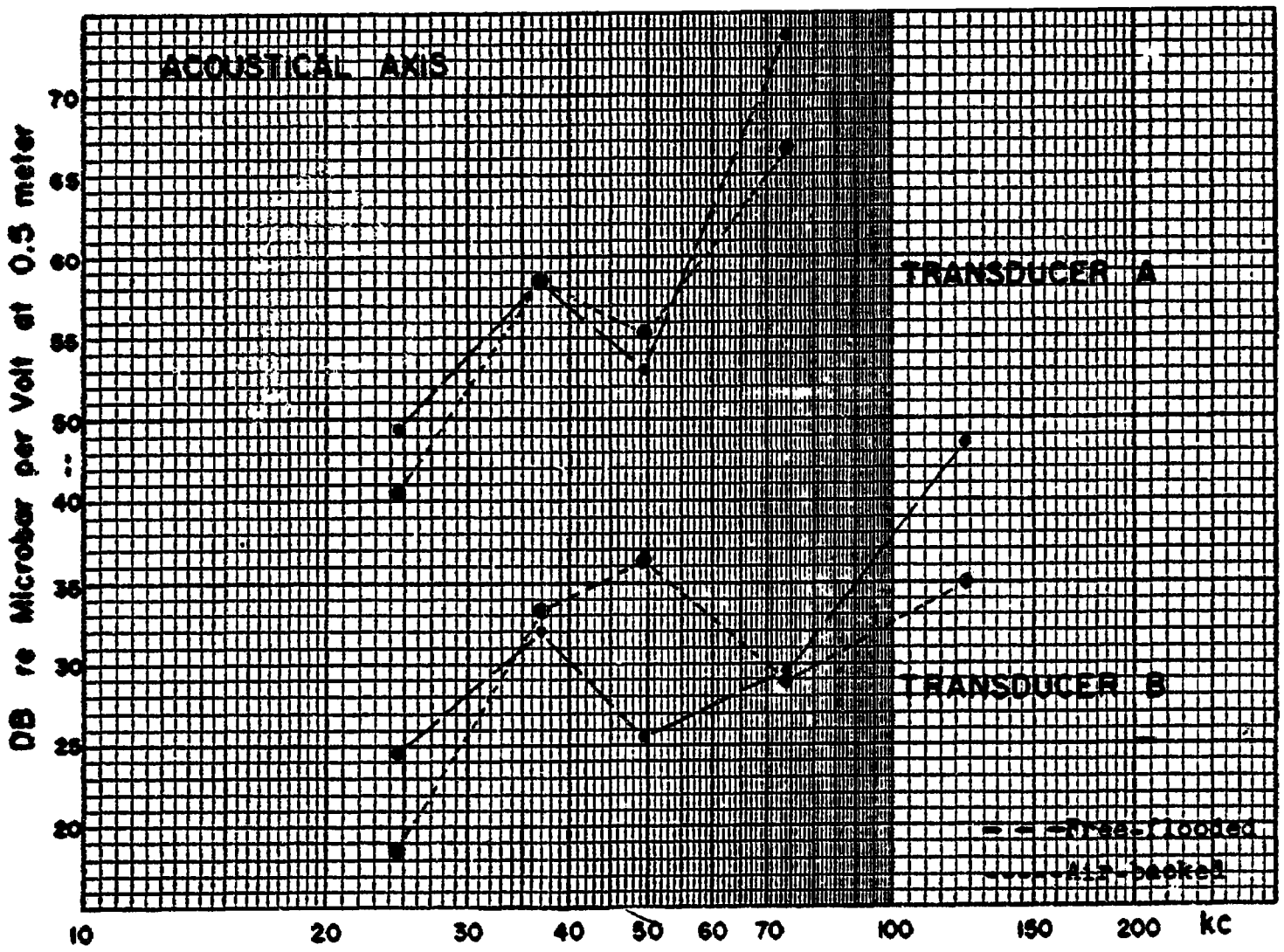

FIG. 9a TRANSMITTING RESPONSE OF TRANSDUCERS A & B

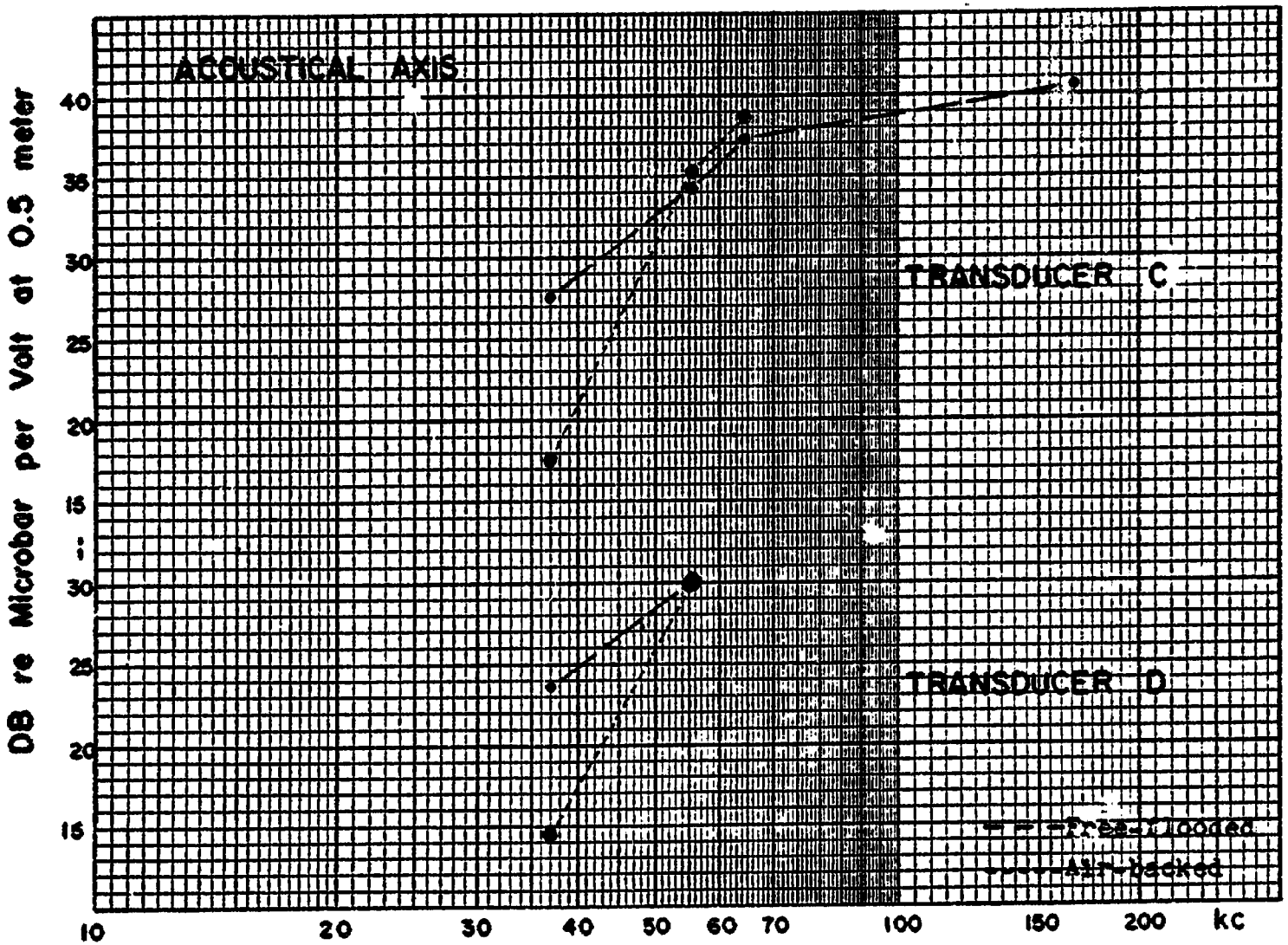

FIG. 9b TRANSMITTING RESPONSE OF TRANSDUCERS C & D

The frequencies of interest for transducers A and B are 24.65, 37, 49.4, 74 and 123.3 kilocycles per second, representing values of ka (k is the wave number and a is the radius) of 2, 3, 4, 6, and 10. For transducers C and D, they are 37, 55.5, 74 and 166.5 kilocycles per second, representing values of ka of 2, 3, 4, and 9. The patterns at these frequencies are obtained when possible for both the free-flooded and air-backed cases and plotted together for comparison. Figures 10 to 24 show a complete collection of radiation patterns presented in a format suitable for comparison.

Finally, the total power output at the frequencies mentioned above is computed from the combined knowledge of the absolute transmitting response at one frequency and the polar pattern at the same frequency as the cylindrical axis of the ring rotated. The formula for computing the total power output is

$$P = \frac{1}{\rho_o c} \int\int p^2 \, dS$$

where p is the pressure at the surface on which the power is to be computed. Employing the property that the ring has rotational symmetry about its cylindrical axis, a computer program has been written for automatic computation of the total power output at each frequency on the IBM 1410-FO-970 Operating System. (See Appendix.) The results are shown in Table I.

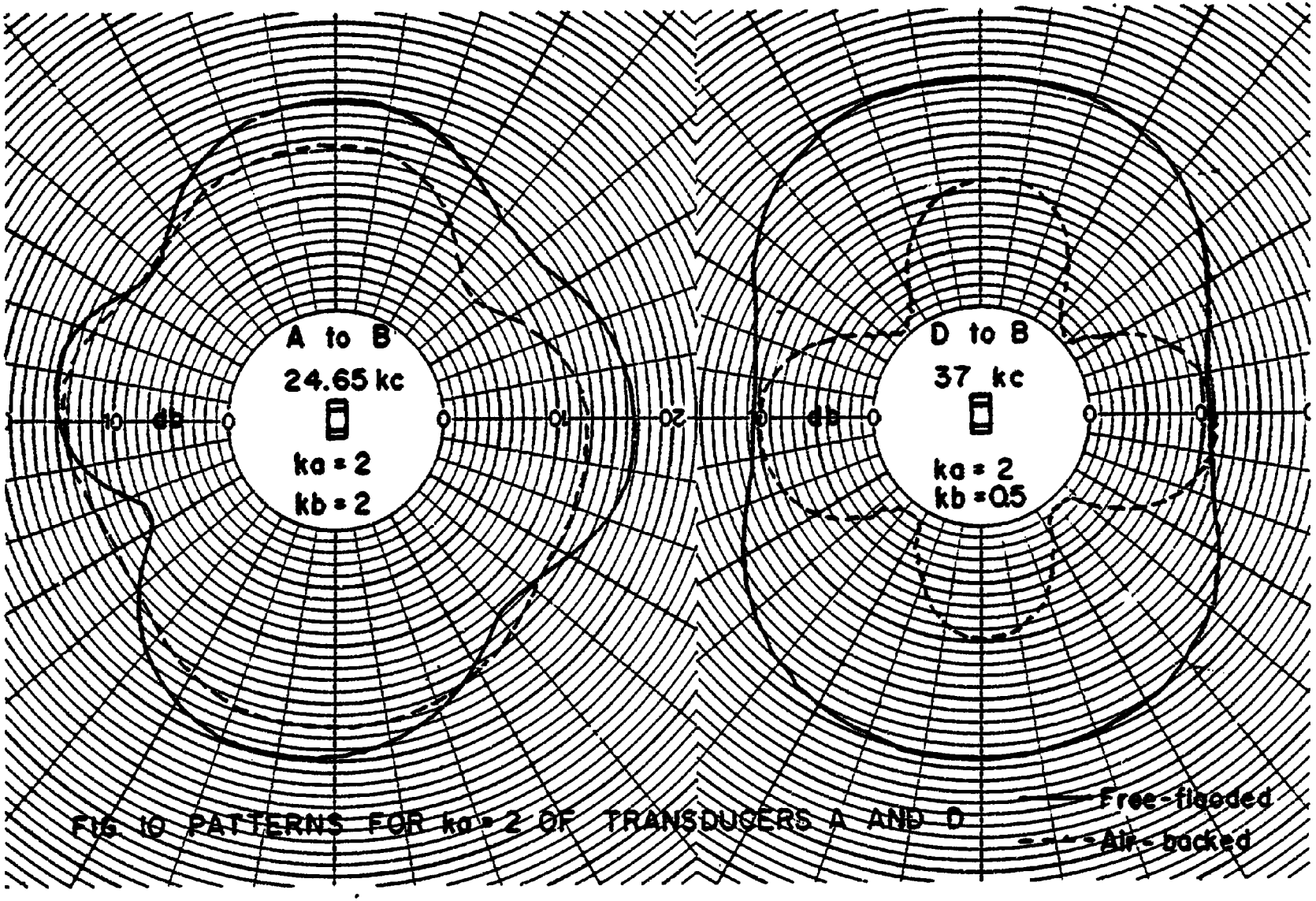

FIG 10 PATTERNS FOR ka = 2 OF TRANSDUCERS A AND D

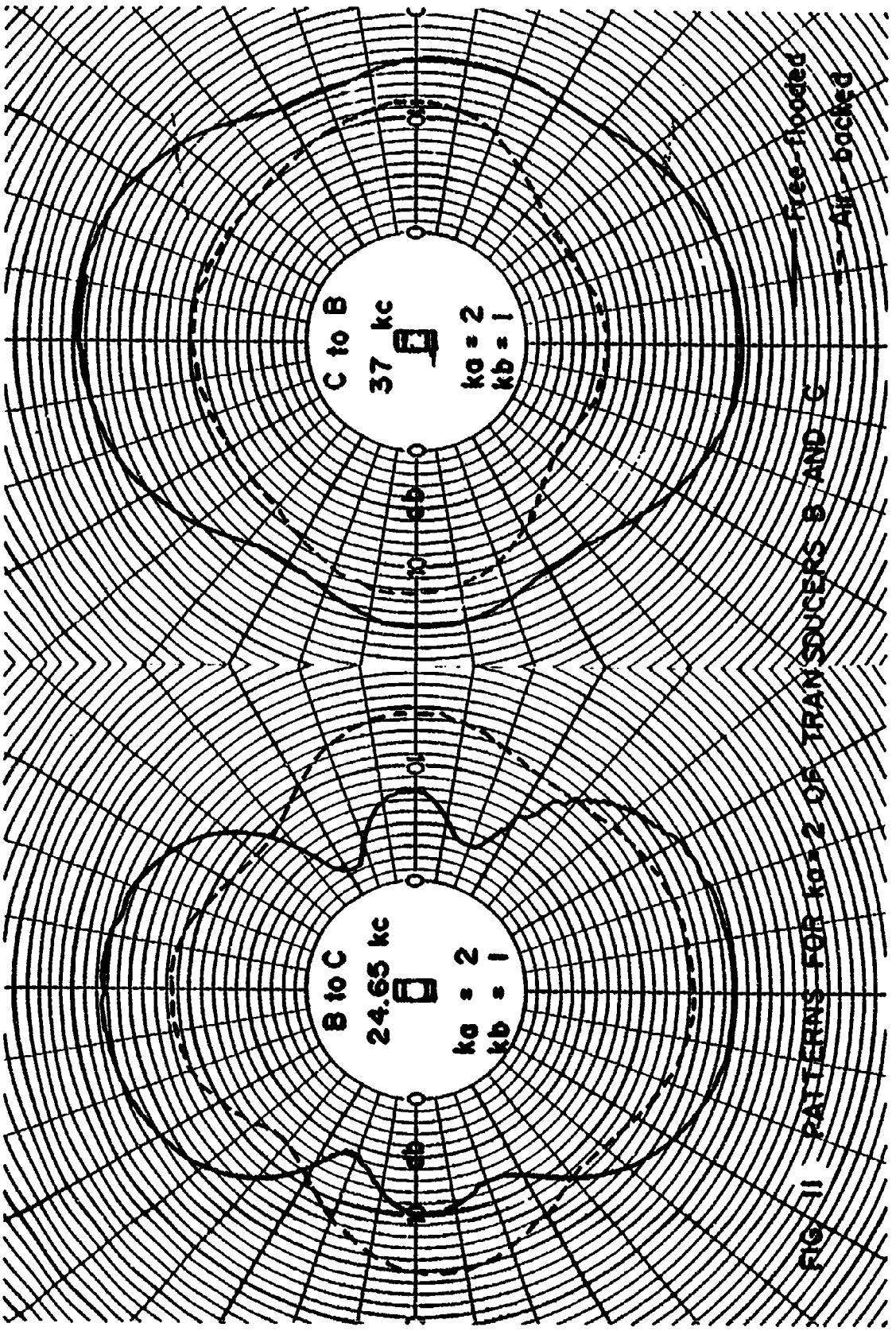

FIG. 11 PATTERNS FOR ka = 2 OF TRANSDUCERS B AND C

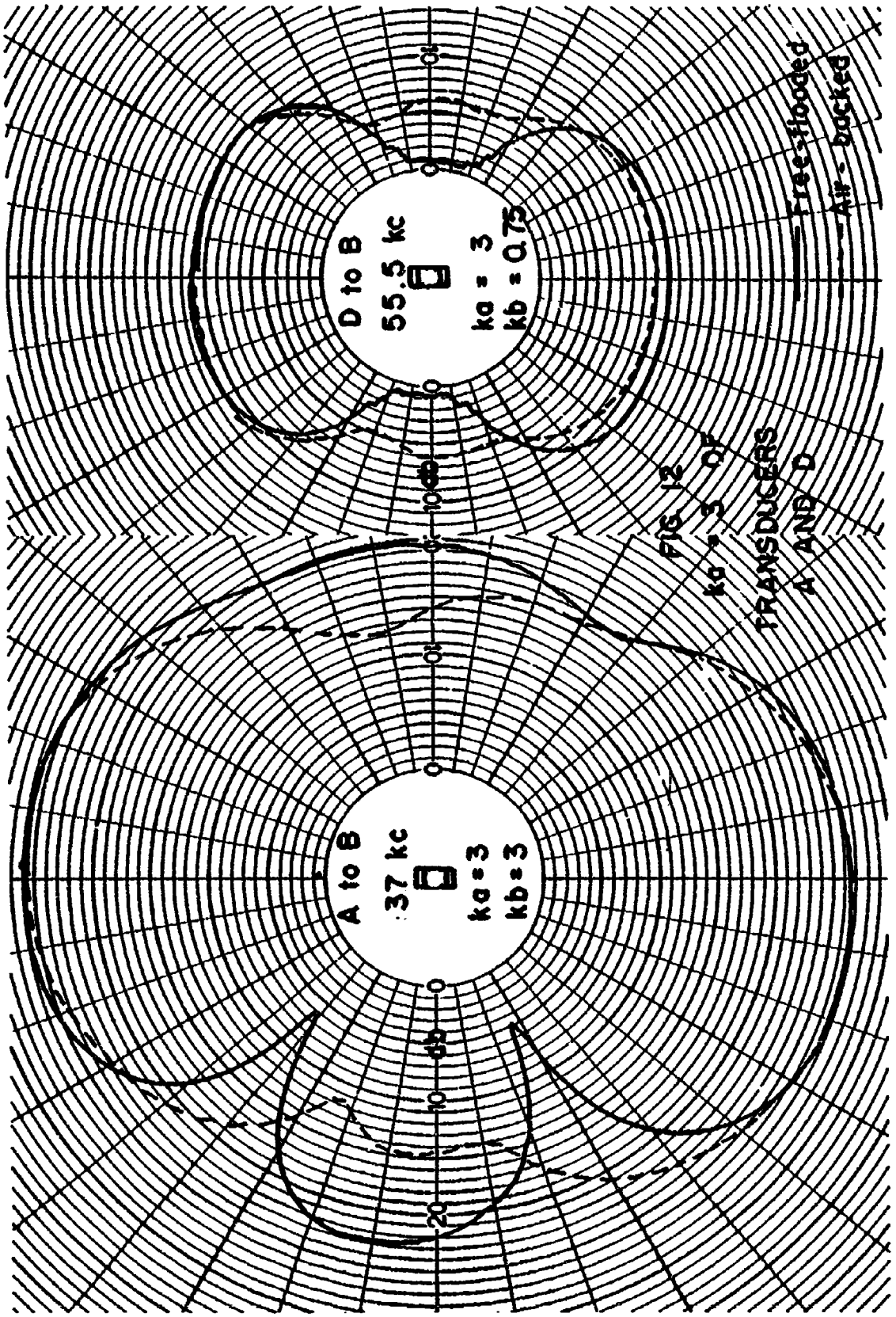
A to B
37 kc
ka=3
kb=3
D to B
55.5 kc
ka = 3
kb = 0.75
0 dB
10 dB
20 dB
FREE-FLOODED TRANSDUCERS A AND D
ka = 3 AT 37 kc
Air - backed
Free-flooded

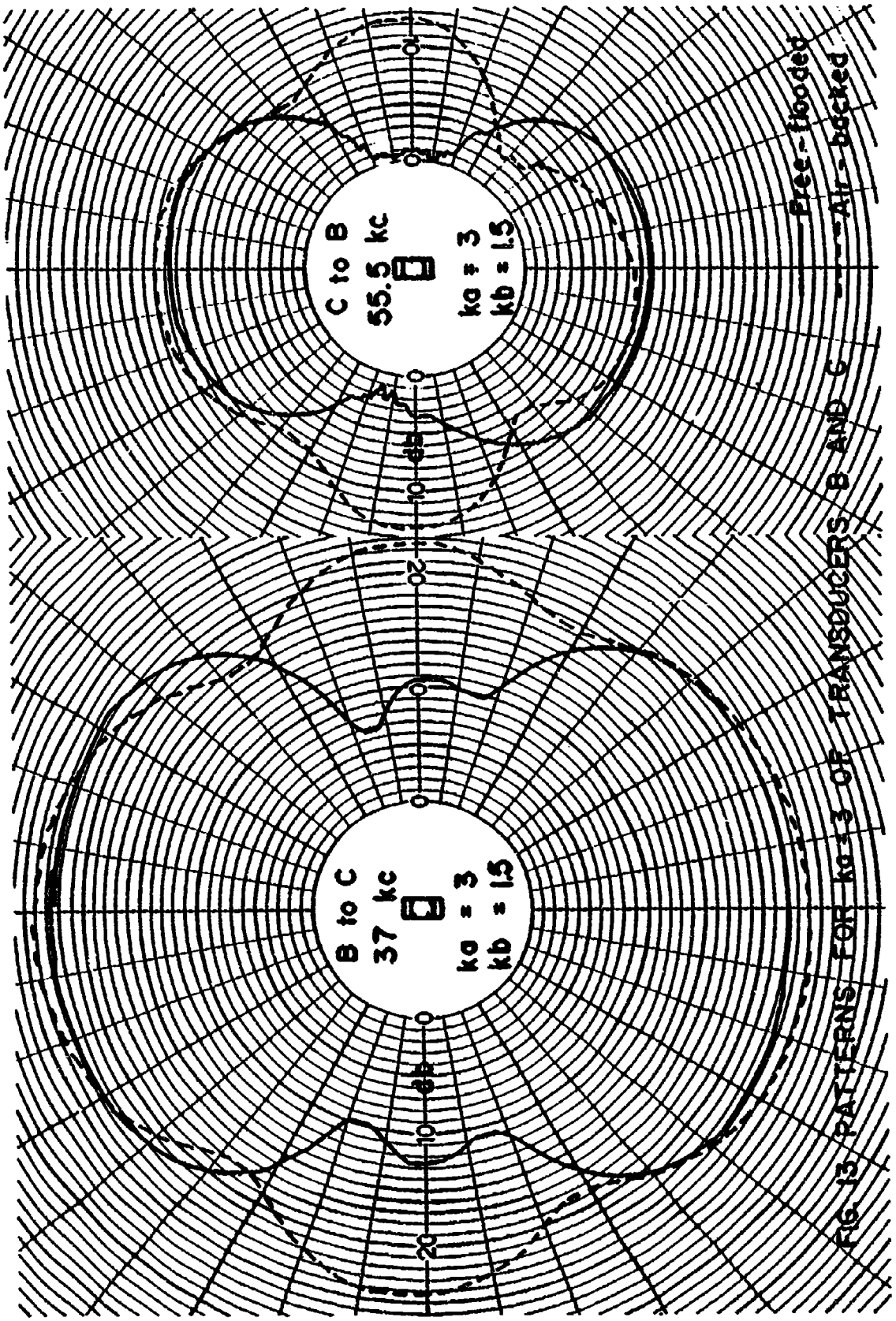

FIG. 13. PATTERNS FOR ka = 3 OF TRANSDUCERS B AND C

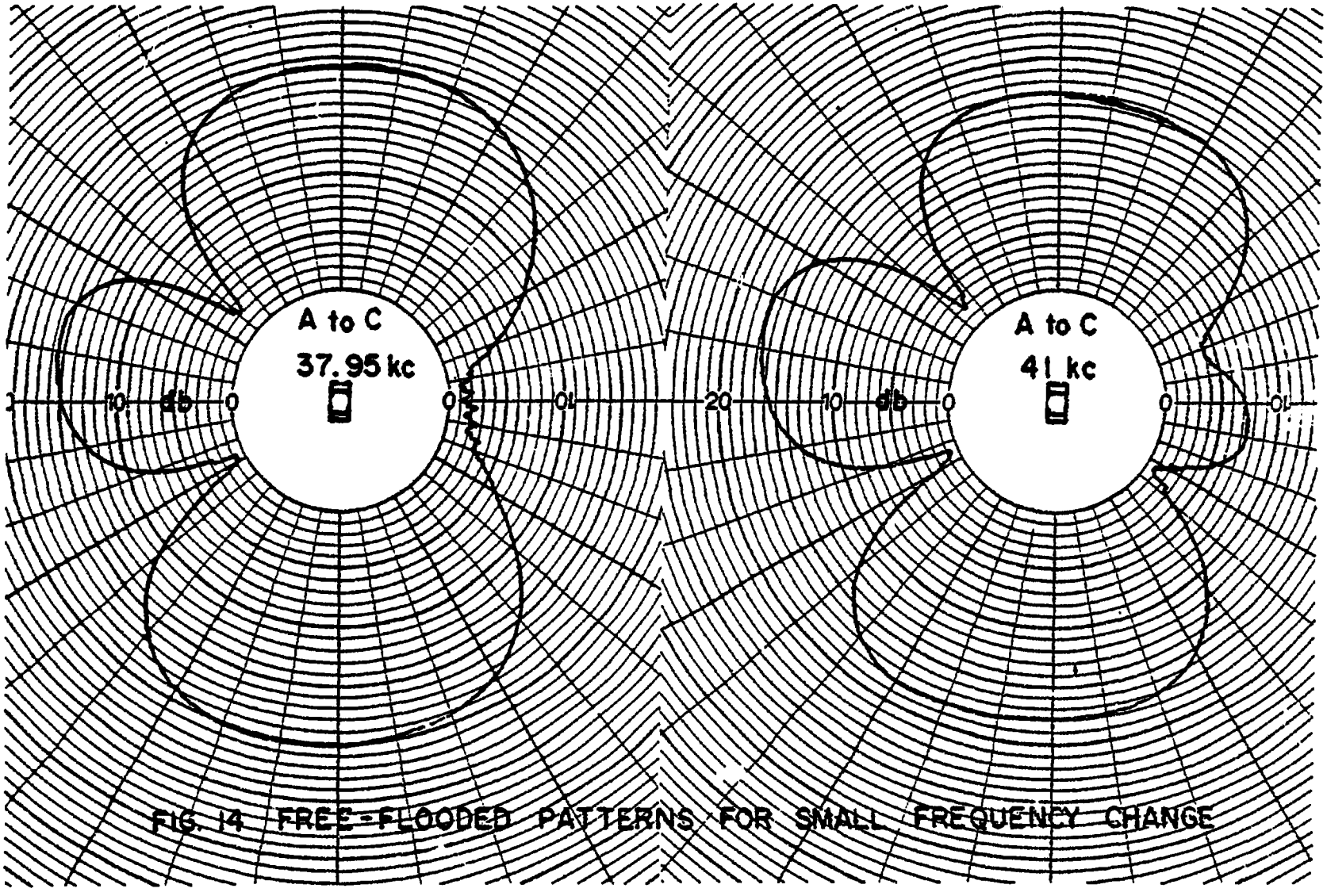

FIG. 14 FREE-FLOODED PATTERNS FOR SMALL FREQUENCY CHANGE

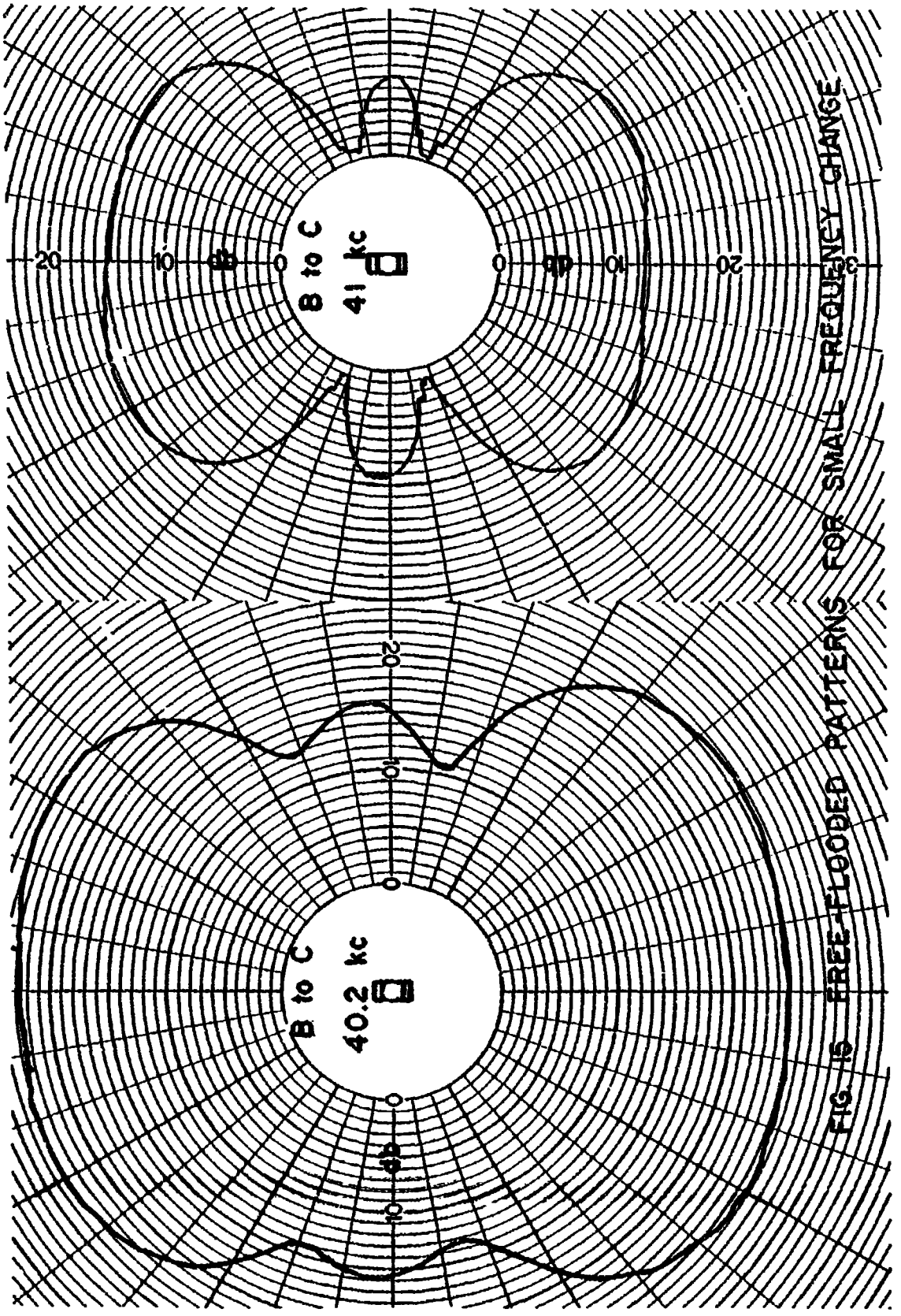

FIG. 15 FREE-FLOODED PATTERNS FOR SMALL FREQUENCY CHANGE

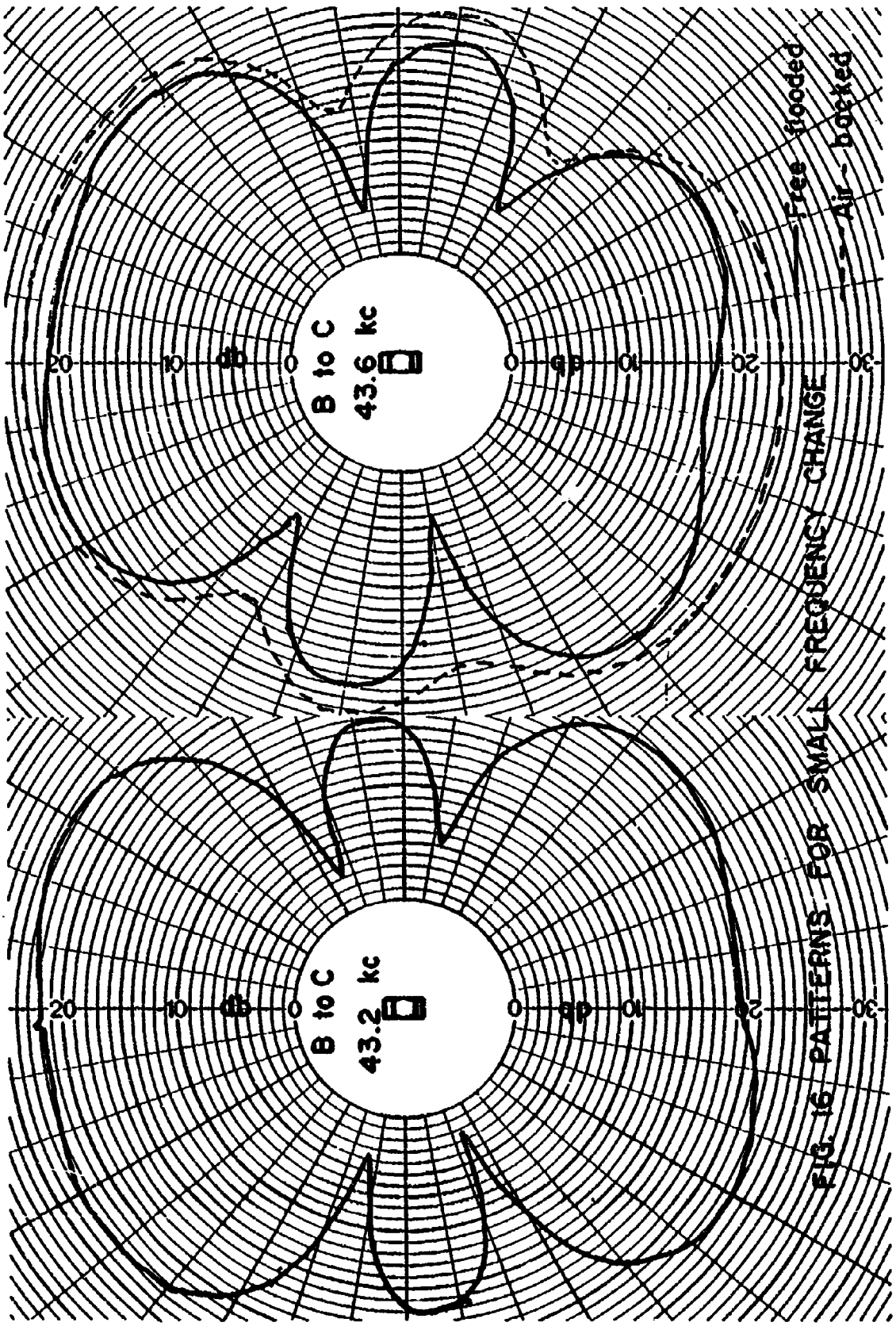

FIG. 16. PATTERNS FOR SMALL FREQUENCY CHANGE

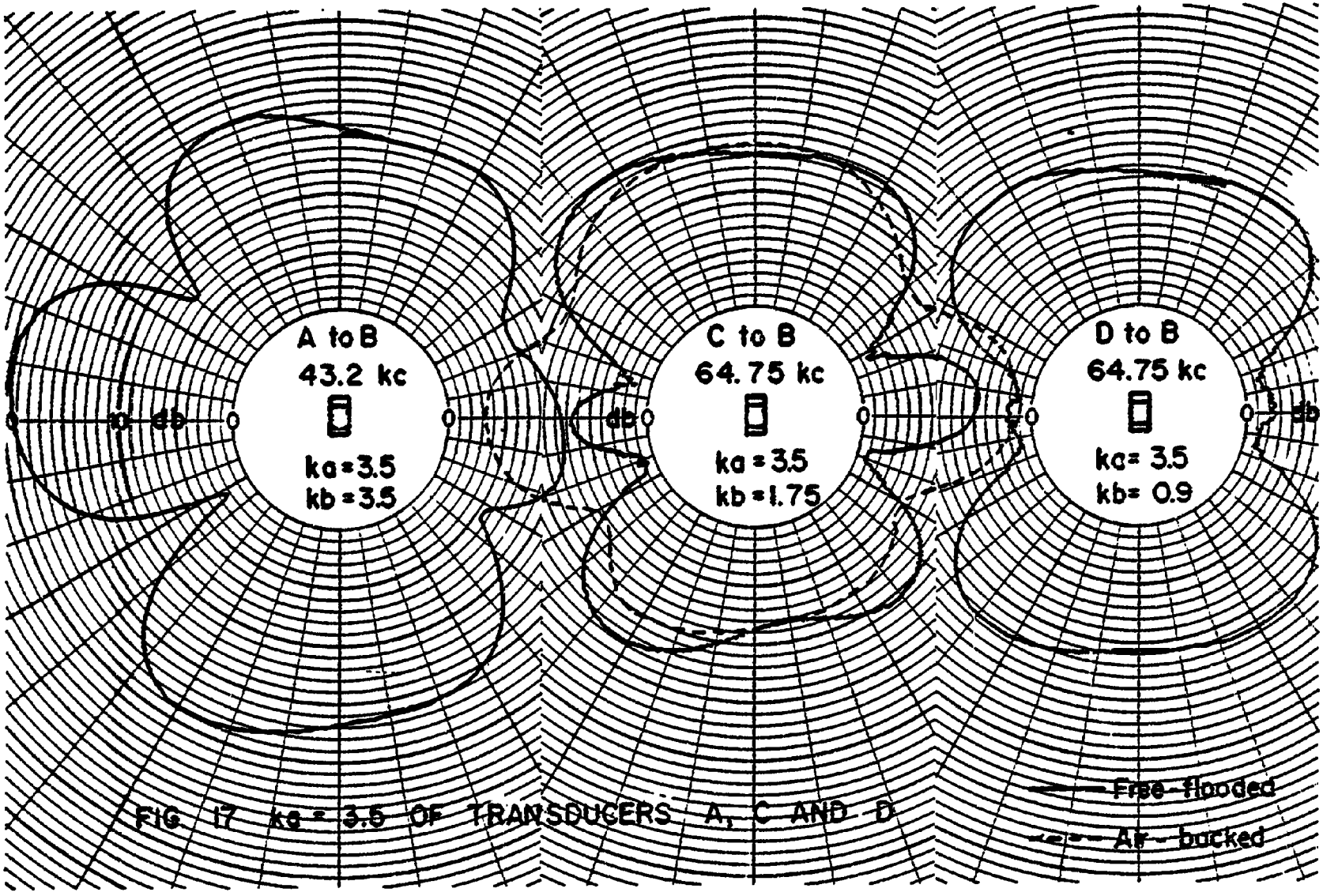

FIG 17 ka = 3.5 OF TRANSDUCERS A, C AND D

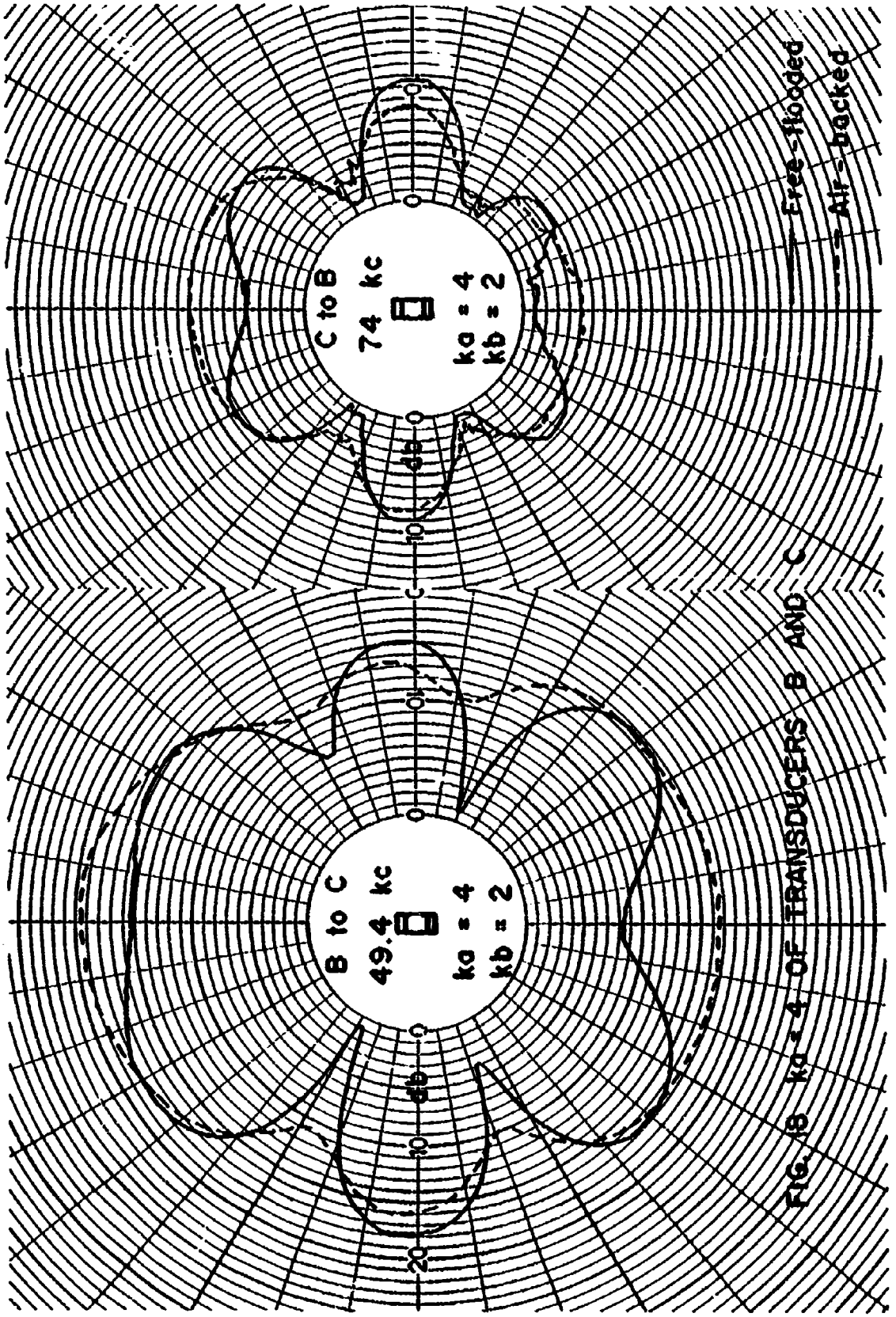

FIG. 18 ka = 4 OF TRANSDUCERS B AND C

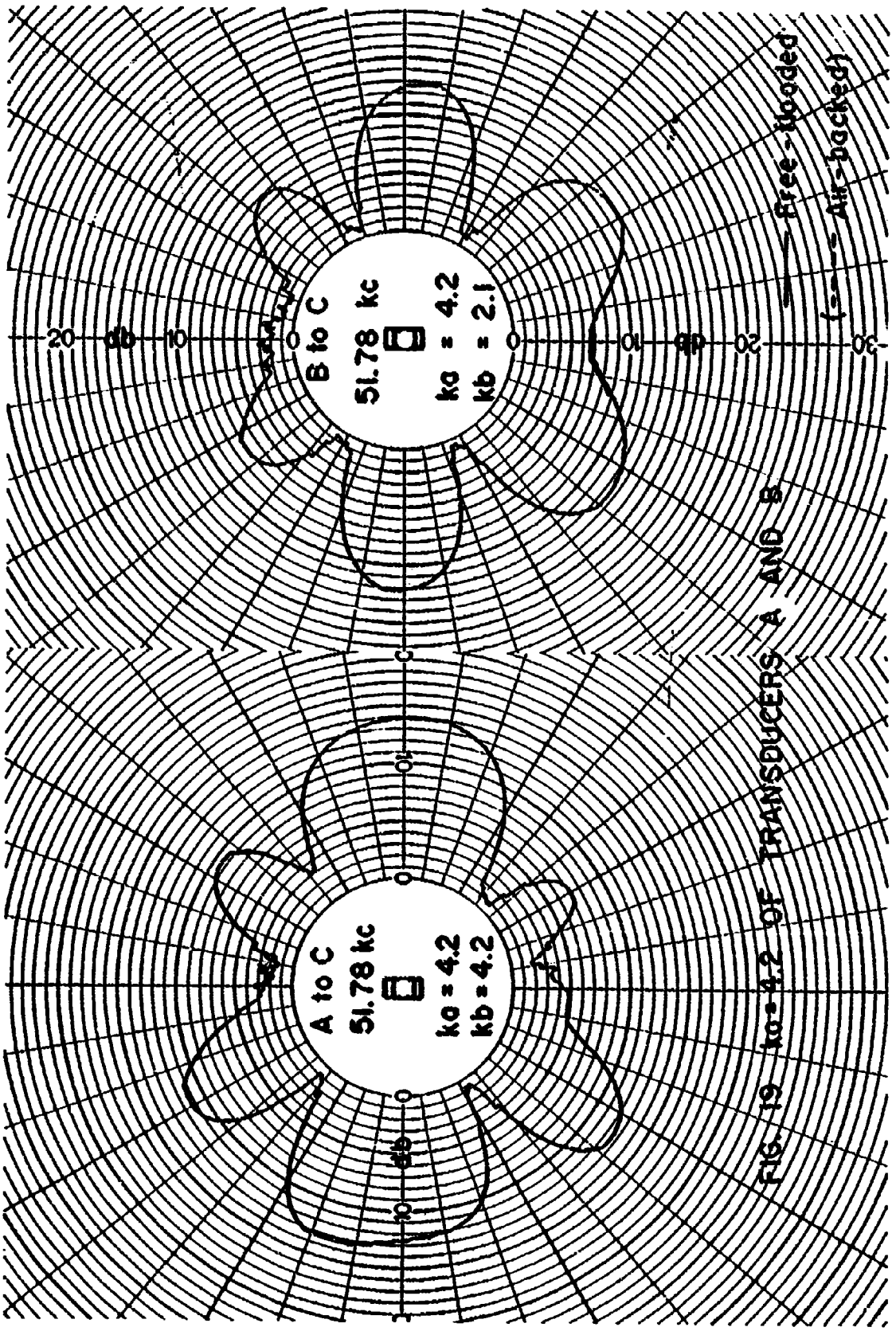

FIG. 19 ka = 4.2 OF TRANSDUCERS A AND B

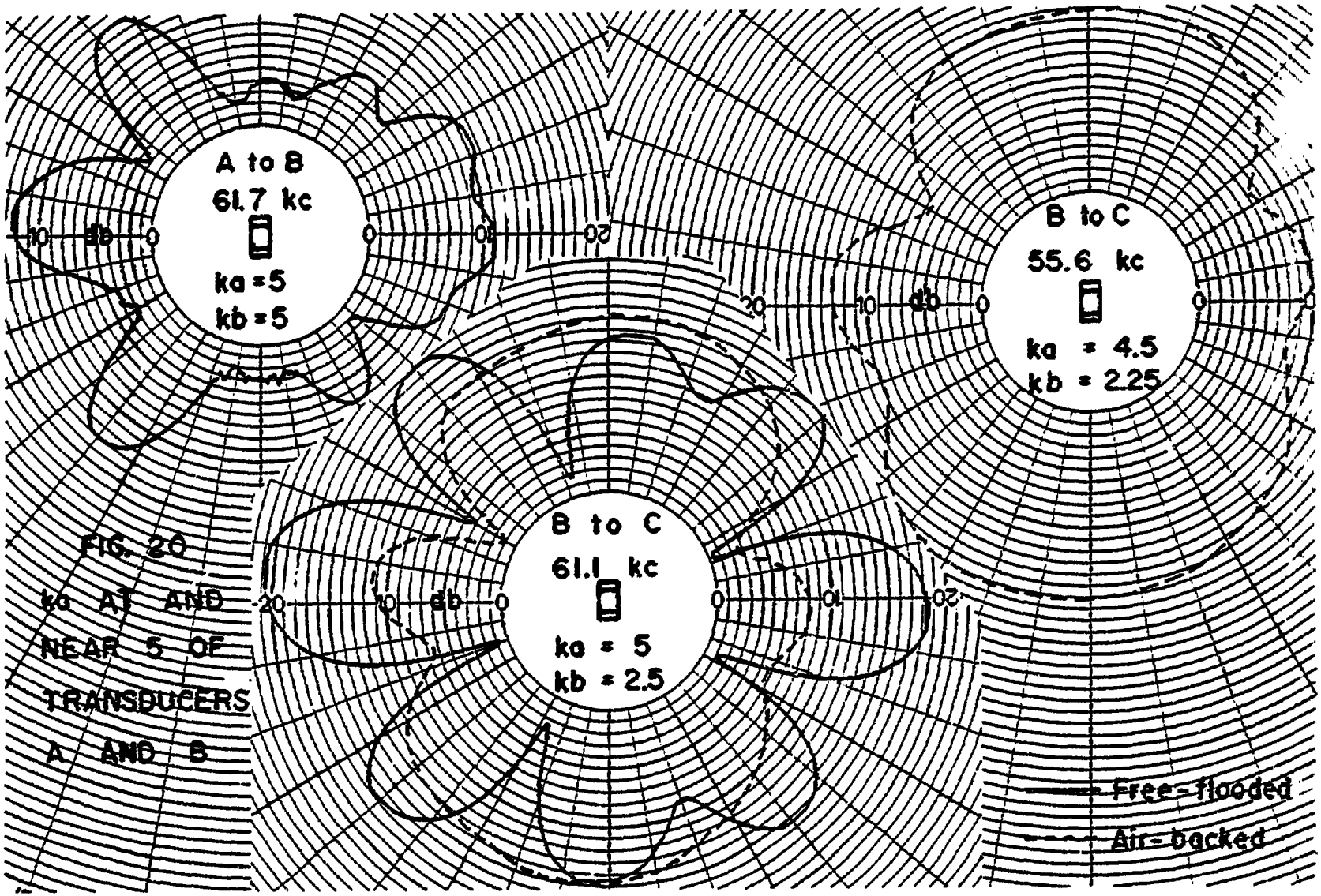

FIG. 20

ka AT AND NEAR 5 OF TRANSDUCERS A AND B

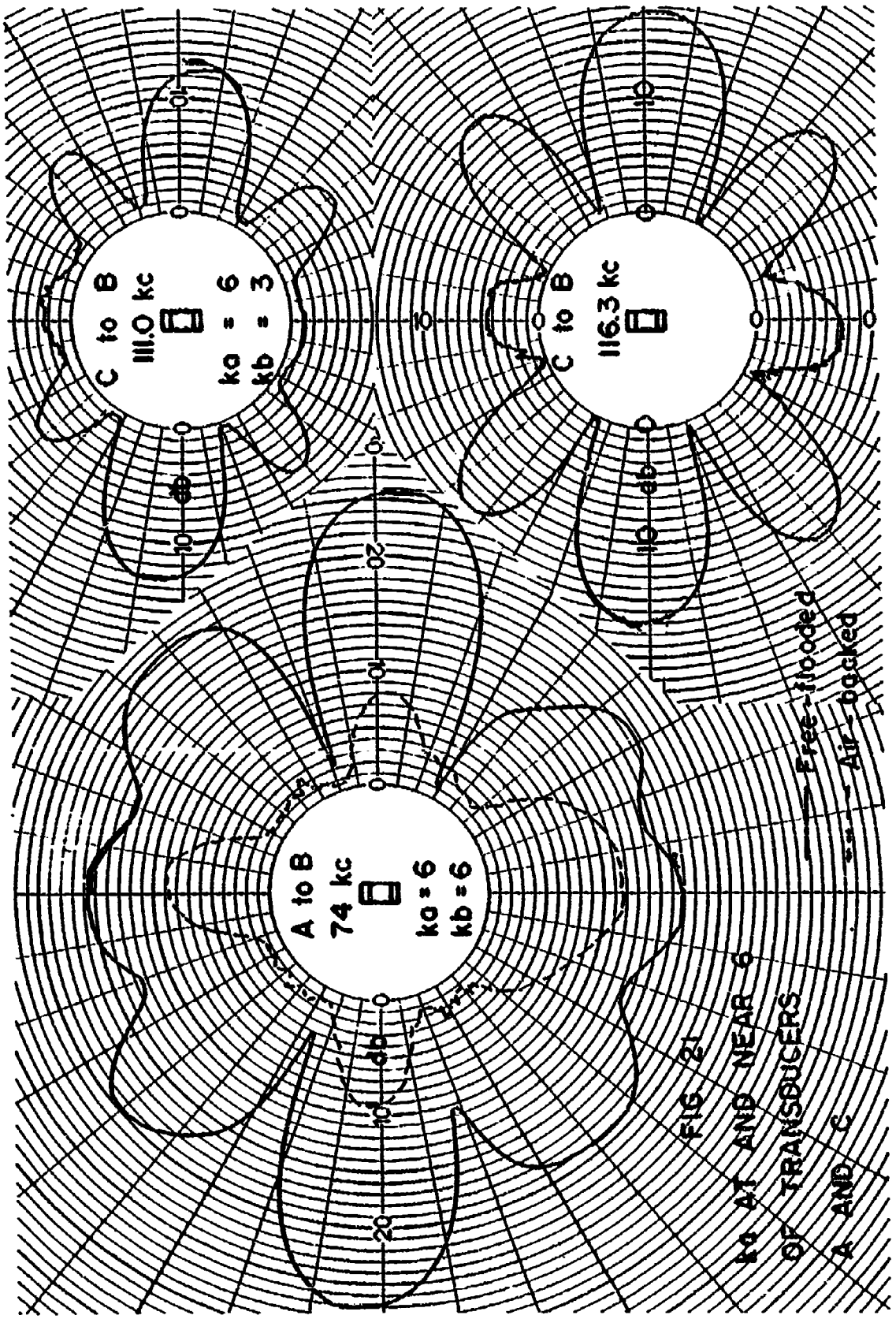

FIG. 21
KA AT AND NEAR 6
OF TRANSDUCERS
A AND C

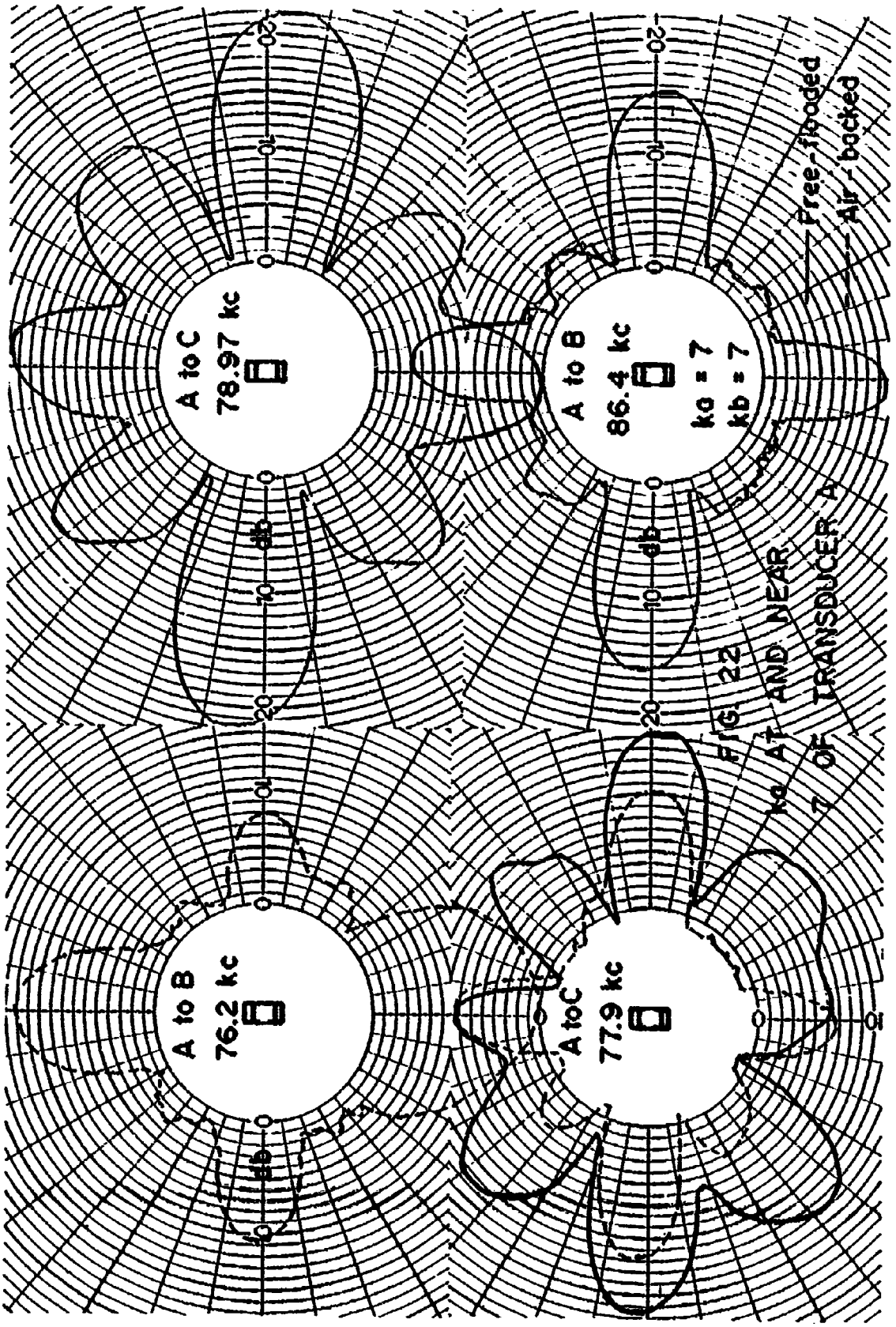

FIG. 22 ka AT AND NEAR 7 OF TRANSDUCER A

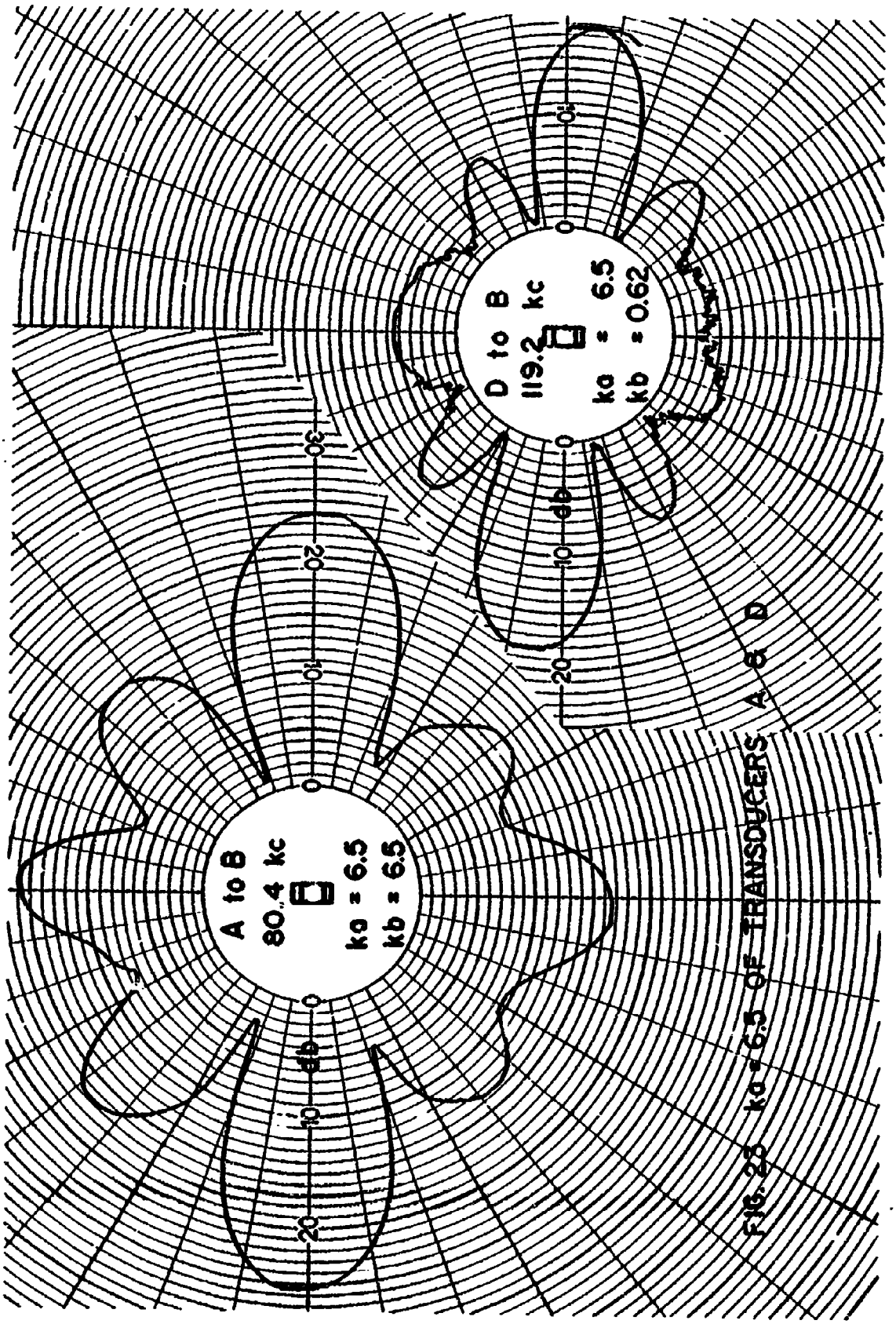

FIG. 20 ka = 6.5 OF TRANSDUCERS A & D

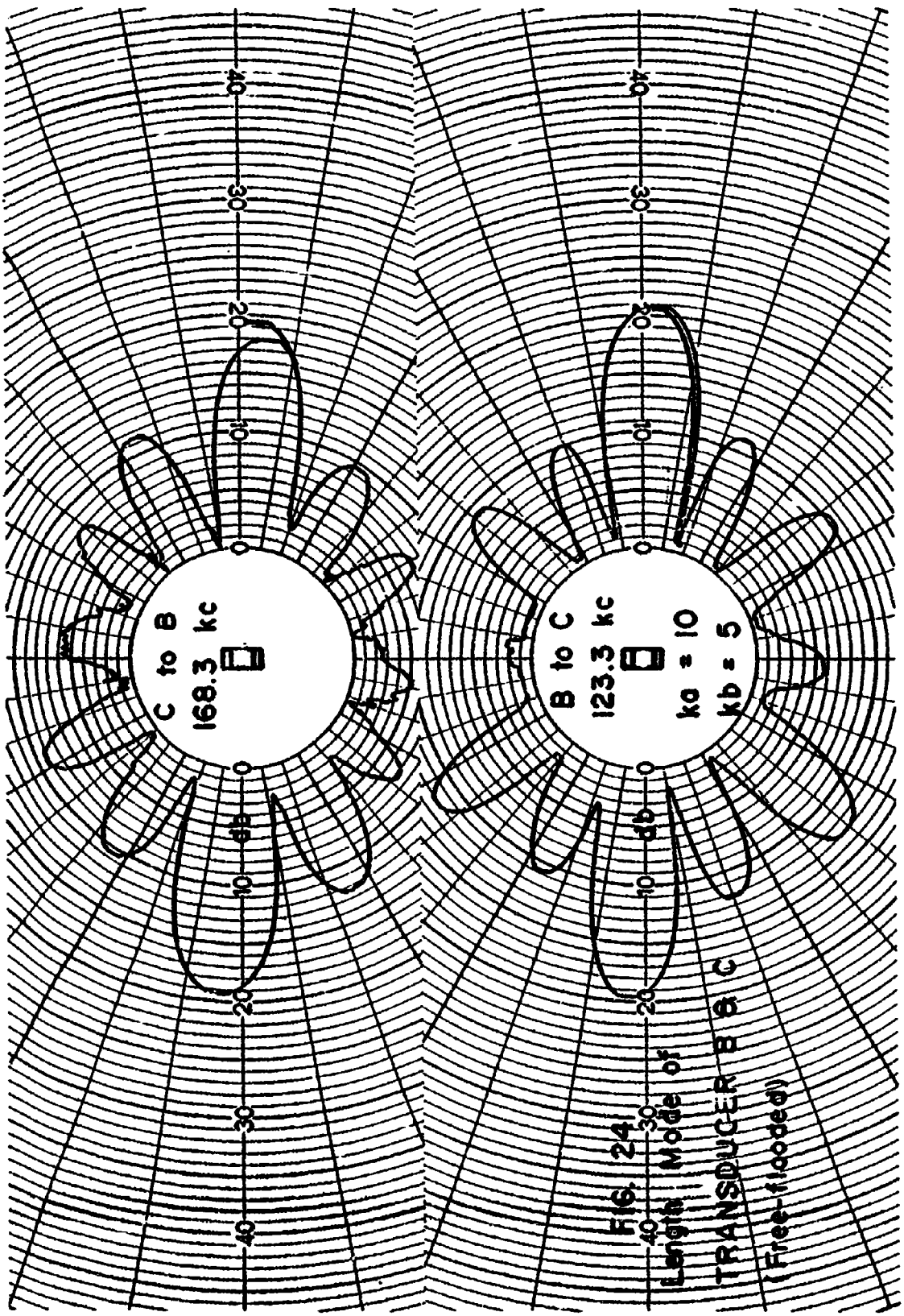

FIG. 24 Length Mode of TRANSDUCER B & C (Free-flooded)

TABLE I

Total Power Output of Ceramic Transducers

ka	TOTAL POWER OUTPUT IN MILLIWATTS PER VOLT DRIVING							
	TRANS. A (ℓ/D=5/6)		TRANS. B (ℓ/D=1/2)		TRANS. C (ℓ/D=1/2)		TRANS. D (ℓ/D=1/4)	
	FL	AIR	FL	AIR	FL	AIR	FL	AIR
		24.65 KC				37 KC		
2	16.3	9	1.2	0.42	1.7	0.31	0.38	0.035
		37 KC				55.5 KC		
3	82	74	4.35	5.5	5.6	8.33	1.0	0.97
					64.75 KC			
3.5					15	13.4		
	74 KC							
6	1040	580						
					168 KC			
9					7			
			123.3 KC					
10			31					

FL denotes free-flooded case and AIR denotes air-backed case.

V

DISCUSSION OF RESULTS

From the impedance curves of Figures 7a-d, one can first distinguish the different resonance modes of each ring. Approximately one has:

Resonance mode	A	B	C	D
Radial	38 kc	38 kc	60 kc	60 kc
Length	76 kc	125 kc	180 kc	---

Note that the length mode of transducer D does not appear in our frequency range, the calculated resonance being 400 kc. Off resonance, the water-flooded rings have nearly the same impedance characteristics as when they are free to vibrate in air. At resonant points however, the impedance changes considerably, especially at the radial resonance, an expected effect attributed mainly to the water column inside the ring. As expected also, the mass of the water causes the resonant frequencies to drop slightly.

A third dip which occurs at 140 kc for all four rings is due to an extraneous electrical circuit resonance and should be ignored, as indicated by the dashed lines on the curves.

Besides the two main resonances, radial and length, a third mode which cannot be neglected in the study of the ring's behavior is a mode resulting from the vibrating of the water column in the ring,

often called the "squirter" mode. This is a complicated vibration studied first by Rayleigh and Helmholtz and recently by various authors. Yet a useful theoretical prediction of this resonant frequency is still not available. In reference 16, Merriweather suggested an empirical formula derived from his experimental data for calculating the frequency of the $(2n-1)\lambda/2$ squirter resonances of cylinders without any form of pressure-release. This formula,

$$f = \frac{(2n-1)\ c}{2(1.257\ \ell + 2a \times 0.526)} ,$$

is used to calculate the first three squirter resonances of the four rings. They are given in Table II.

TABLE II

Squirter Resonances

Ring	Fundamental (λ/2)	3λ/2	5λ/2
A	12.7 kc	38 kc	63 kc
B	17.5 kc	53 kc	87.5 kc
C	26 kc	78 kc	130 kc
D	28 kc	83 kc	140 kc

These frequencies are very pertinent in the following discussion of the rings' behavior described by means of their response curves and radiation patterns.

The receiving characteristics in Figures 7a-d, though different from the true response curves because of the frequency dependence of the impedance and the reciprocity constant, serve to indicate the variation of the responses of the rings on the acoustical and cylindrical axes. The 37 kc point on these curves are absolute response levels since the reciprocity calibration was made at this frequency.

In Figure 7a, one notes that the acoustical axis response at radial resonance (38 kc) is the same for both the free-flooded and the air-backed cases as expected. On the cylindrical axis however, while the air-backed cylinder was expected to have better response at the same frequency, it does not. This is due to the interaction of the $3\lambda/2$ squirter mode which is near the same frequency. The length mode stands out distinctively at the 76 kc with the free-flooded response 8 db greater on the acoustical axis and 20 db greater on the cylindrical axis relative to the air-backed response. This is due to the better coupling with water in the free-flooded case and the effect of the higher order squirter modes. It is unfortunate that the pulse technique and the lack of receiver sensitivity precluded extending these tests below 20 kc, where the important fundamental circumferential mode of vibration arises (i.e. ka = 1 at 12.3 kc for ring A).

In Figure 7b, one sees similar patterns for ring B, in the radial mode; acoustical axis response is the same for the two cases (air and water backed) and the cylindrical axis response is stronger in the air-backed case. The $3\lambda/2$ squirter mode is seen at 53 kc. The length

mode is at about 120 kc and the difference between the free-flooded and air-backed cylindrical axis responses is reduced to 14 db. This is probably due to the weaker squirter action from the shorter vibrating water column in B.

Figures 7c and 7d show more of the same behavior. The acoustical axis responses are equal at the radial resonances and the free-flooded cylindrical axis responses are affected by the high order squirter modes. Note that the relative strength between the cylindrical axis responses of the two cases decreases as the rings become shorter.

Figures 9a-b give an idea of the absolute transmitting response of the cylinders. The acoustical axis responses at frequencies of interest are calculated from the receiving characteristics curves. For A, these frequencies represent approximate ka values of 2, 3, 4 and 6; for B, 2, 3, 4 and 10; for C, 2, 3, 3.5 and 9; and for D, 2 and 3. The differences between the free-flooded and air-backed responses are the same as in the curves of Figures 7a-d, but the absolute magnitudes are not. These absolute magnitudes are used together with the radiation patterns at these same frequencies in a computer program (see Appendix) to calculate the total power output of the cylinders for one volt drive (Table I).

The polar radiation patterns in Figures 10-24 provide much more insight into the behavior of the rings. As a general rule, the discussion will be made in terms of the parameters ka and kb together with the different squirter mode frequencies. The justification for this lies in the fact that the combined effect of ka and kb, when not affected by the squirter action, is the same even for different dia-

meter rings (B and C) as shown by the resemblance of the patterns in Figures 11, 13, 18 and 24.

Comparing Figures 10 and 11 where ka is 2 throughout, one notes that for the free-flooded case on the cylinder axis ring A has from 5 to 8 db more output than ring B for the same acoustical axis response. This is probably due to the fact that A is twice as long as B, causing the combined radiation from inside and outside the ring to be constructive and thus stronger. This effect is not so strong in rings C and D, yet at this frequency (37 kc), the fundamental squirter mode comes into effect and helps make the cylindrical axis response strong (especially ring C). In the air-backed case, the effect of the back of the ring is eliminated and the patterns are almost alike and omnidirectional except for the shortest ring D where there are four distinct, symmetrical lobes. This is likely due to the approximate equality of the total radiating areas of the two ends and the cylindrical surface, causing a constructive effect near the cylindrical axis and a destructive effect at 45° angles.

A comparison of the total output power at this ka value (Table I) shows that the free-flooded case generally gives more output power than the air-backed case, the difference increases as the rings become shorter or the length-to-diameter ratio becomes smaller. Note that ring C is an exception since it is being affected by the fundamental squirter mode.

Figures 12 and 13 show the patterns near each ring's radial resonance. The ka value here is 3. At 37 kc, ring A has reached the next higher order squirter mode ($3\lambda/2$, f= 38 kc) while ring B has not. The distortion of the right side of the pattern for A is due to the

clamping action of the connecting cable. This conclusion is supported by the patterns for slightly higher frequencies in Figure 14. Here, the squirting action stays the same while the distortion changes in shape. The free-flooded patterns of rings C and D near radial resonance resemble a figure eight where the cylindrical axis responses have nearly disappeared due to the destructive interference from the sides. The patterns for the air-backed case are similar for all four rings although the cylindrical axis responses of A and D are 5-8 db less than the acoustic axis responses. It is noted that the acoustic axis response is approximately the same in both free-flooded and air-backed cases as mentioned before.

Refering again to Table I, the air-backed cylinders at this ka value in general give more output power than when free-flooded. The exception in A is again due to the coincidence with the $3\lambda/2$ squirter mode.

In Figure 17, the patterns for ka $\cong$ 3.5, representing a small increase in ka value from the previous case, are shown. One sees similar effects here. The $3\lambda/2$ squirter mode is still interfering with the radial mode in A giving fair cylindrical axis response. For C and D, (squirter mode at 78 kc and 83 kc respectively) it has only begun, causing the same effect on the cylindrical axis output. The flattening of the lobes on the acoustical axis indicates that a higher order mode is about to take over. The output power of the free-flooded ring C has become slightly stronger than the air-backed case at this frequency.

Figures 18 and 19 show the free-flooded patterns of A, B, and C at ka values of 4 and 4.2. Here they have broken into distinct lobes.

Theoretically the number of lobes should be twice the ka value, but in this case the high order squirter mode causes the two lobes near the cylindrical axis to combine into one larger lobe.

The argument can be used to explain the shape of the remaining patterns of higher ka values in Figures 20-24. The length and high order squirter modes are the main modes of vibration, causing the patterns to have a flattened shape with strong output on the cylindrical axes. At these high frequencies, the air-backed response has decreased considerably, moreso on the cylindrical axis. Note that the patterns have become extremely symmetrical since the extraneous interferences due to mechanical loading, clamping, etc., have become negligible.

In general, the radiation patterns have relatively unchanging shape for a frequency variation as large as one octave. This is noted from patterns taken at frequencies close together and at different times as shown in Figure 14, 15, 16, 21 and 22. Thus one can usually predict the general shape of the patterns within an octave range of frequency knowing the mode or modes of vibration of the ring.

VI

CONCLUSIONS

This paper has presented a review of the existing theoretical studies of finite cylinders and has evaluated their advantages and disadvantages. It was found that the approximate solution by R. S. Haas and F.H. Middleton using the iteration technique most useful for practical purposes.

It has been shown that a design parameter study can be made successfully in the laboratory by using the scale modeling technique. The results of this study include impedance characteristics, calibration curves (using the reciprocity principle), total output power and radiation patterns of four different rings, each in the free-flooded and air-backed configurations.

From the data, the following conclusions can be made about the behavior of finite cylinders:

a. When devoid of all forms of pressure-release underwater, the ring is damped considerably at resonances compared to when it is free to vibrate in air, due mainly to the water column inside the ring.

b. If the driving voltage is kept constant for the whole frequency range, the output at different axes of the ring depends mainly on three factors -- the values of ka, kb and the thickness-

to-diameter ratio. Also, the "squirter" resonances due to the vibration of the water column inside the ring cause the output on the cylindrical axis in the free-flooded case to be strong at certain frequencies. The longer the ring, the stronger is the squirter mode.

c. In general, the acoustical axis responses in both the free-flooded and air-backed cases are approximately the same when the ring is operating near its radial resonance. On the cylindrical axis however, the Air-backed response is better than the free-flooded response, except when near the squirter resonance. The total output power in the air-backed case is generally more than in the free-flooded case at radial resonance. Off radial resonance the free-flooded rings provide more power than the air-backed rings, the difference increasing as the rings become shorter for the same diameter.

d. As the ka value increases, the patterns acquire more lobes with the number of lobes equal to twice the ka number minus two due to the action of the high order squirter modes. The cylindrical axis response becomes much stronger under the combined action of the length and squirter modes.

To summarize, a finite cylinder may be designed to work properly in many different modes without any form of pressure-release, an asset in deep submergence applications.

VII

APPENDIX

FORTRAN COMPUTER PROGRAM

This Fortran computer program is designed to automatically calculate the total power output of a cylindrical transducer at different frequencies. The transducer must have an axial symmetry (cylindrical axis) and the sound pressure in db must be known from a polar pattern as well as the distance between projector and hydrophone which in this case is 0.5 meter (as in the "RADIUS" statement). The program integrates around the spherical surface from a circle in increments of two degrees. It thus requires four data cards for each computation, on which the frequency and the pressures in db are written. There will be an error message at the end of the computation when all data is exhausted. Please ignore it.

```
C          FORTRAN LISTING    IBM 1410-FO-970
C     POWER OUTPUT OF CYLINDRICAL CERAMIC TRANSDUCERS
C      NGUYEN TRANH CHIEU AUGUST 6 1964
      DIMENSION DB(50)
      COMMON FREQ
    1 FORMAT (F6.0)
    5 FORMAT  (18F4.1)
    2 FORMAT(2F20.4)
   10 READ (1,1) FREQ
      READ (1,5)(DB(I), I = 1,45)
      PHI= -3.1416/180.
      POWERO = 0.0
      RHOCI = 1.48E06
      DELTAL=-PHI
      DO 20 I = 1,45
      PRESS = (10.**((DB(I))/20.))/10.
      SQPRES = PRESS*PRESS
      PHI=PHI+2.*DELTAL
      RADIUS = .5*COS(PHI)
      AREA = 2.*3.1416*RADIUS*DELTAL
      POWER1 = AREA*SQPRES/RHOCI
   20 POWERO=POWERO+POWER1
      POWERO=POWERO*2.
      WRITE(3,2) FREQ, POWERO
      GO TO 10
      STOP
      END
```

REFERENCES

1. Roske, "The Development of an Ultrasonic Transducer Using a Barium Titanate Ceramic", Master's Thesis, University of Rhode Island, 1954.

2. D. T. Laird and H. Cohen, "Directionality Patterns for Acoustic Radiation from a Source on a Rigid Cylinder", Journal of the Acoustical Society of America, 24, 46, 1952.

3. Philip M. Morse, Vibration and Sound, McGraw-Hill Book Co., Inc., p. 297, 1952.

4. G. A. Brigham and M. F. Borg, "Sound Radiation from a Finite Cylindrical Shell with Rigid End Caps", General Dynamics Corp., Electric Boat Div., Tech. Mem. SV59-g, (October, 1959).

5. D. H. Robey, "On the Radiation Imedance of an Array of Finite Cylinders", The Journal of the Acoustical Society of America, 27, 1955, p. 706.

6. Morse and Feshback, Methods of Theoretical Physics, Vol. 1, New York: McGraw-Hill Book Co., Inc., p. 804, 1953.

7. C. H. Papas, Journal of Mathematical Physics, 28, p. 227, 1950.

8. D. H. Robey, "On the Radiation Impedance of the Liquid-Filled Squirting Cylinder, The Journal of the Acoustical Society of America, 27, p. 711, 1955.

9. N. G. Parke III and W. Williams, Jr., "Mathematical Methods in Transducer Field Theory: The Finite Cylinder", The Parke Mathematical Laboratories, Inc., 1962.

10. Ibid, page 10.

11. L. H. Chen and D. G. Schaveikert, "Sound Radiation from an Arbitrary Body", The Journal of the Acoustical Society of America, 35, p. 1626, 1963.

12. Miguel C. Junger, "A Variational Solution of Solid and Free-Flooding Cylindrical Sound Radiators of Finite Length," Cambridge Acoustical Association, Inc., Technical Report V-177-48, 1964.

13. R. S. Haas and F. H. Middleton, "A Deep Water Model of the Flooded Cylindrical Radiator", University of Rhode Island, Technical Report No. 1, Contract NONR-396(12), 1963.

14. Papers given at the 65th and 67th meeting of the Acoustical Society of America.

15. Harold K. Farr, "Radiation from a Free Flooded Spherical Segment," General Instrument Corporation, Harris ASW Division, Westwood, Massachusetts, Internal Memorandum.

16. Anthony S. Merriweather, "The Modes of Vibration in Water of Ferroelectric Cylindrical Tubes Devoid of All Forms of Pressure-Release, U. S. Navy Elec. Laboratory, San Diego, California, Technical Memorandum Number TM-501, 1961.

17. "Free-Flooded Cylindrical Transducers," General Instrument Corporation, Harris ASW Division, Westwood, Massachusetts, Internal Memorandum.

18. Kinsler and Frey, Fundamentals of Acoustics, 2nd Edition, Wiley, page 324.

19. Von H. Kuttruff and P. Wille, "Absoluteichung Verschiedenartiger Wasserschallwandler Im Bereich Von 5 Bis 250 kHz," Acustica, Vol. 12, 1962, p. 410.